FRICTION ANALYSIS IN COLD FORGING

A THESIS SUBMITTED TO
THE GRADUATE SCHOOL OF NATURAL AND APPLIED SCIENCES
OF
MIDDLE EAST TECHNICAL UNIVERSITY

BY

ÖMER NECATİ CORA

IN PARTIAL FULFILLMENT OF THE REQUIREMENTS
FOR
THE DEGREE OF MASTER OF SCIENCE
IN
MECHANICAL ENGINEERING

DECEMBER 2004

Approval of the Graduate School of Natural and Applied Sciences

_____

Prof Dr. Canan ÖZGEN
Director

I certify that this thesis satisfies all the requirements as a thesis for the degree of Master of Science.

_____

Prof. Dr. Kemal İDER
Head of Department

This is to certify that we have read this thesis and that in our opinion it is fully adequate, in scope and quality, as a thesis for the degree of Master of Science.

_____	_____
Prof.Dr. Haluk DARENDELİLER	Prof. Dr. Metin AKKÖK
Co-Supervisor	Supervisor

Examining Committee Members

Prof. Dr. R. Orhan YILDIRIM	(METU,ME)	_____
Prof. Dr. Metin AKKÖK	(METU,ME)	_____
Prof Dr. Haluk DARENDELİLER	(METU,ME)	_____
Prof. Dr. Mustafa İ. GÖKLER	(METU,ME)	_____
Prof. Dr. Can ÇOĞUN	(Gazi University,ME)	_____

I hereby declare that all information in this document has been obtained and presented in accordance with academic rules and ethical conduct. I also declare that, as required by these rules and conduct, I have fully cited and referenced all material and results that are not original to this work.

Name, Last name: Ömer Necati CORA

Signature :

ABSTRACT

FRICTION ANALYSIS IN COLD FORGING

CORA, Ömer Necati
M.S., Department of Mechanical Engineering
Supervisor: Prof. Dr. Metin AKKÖK
Co-supervisor: Prof. Dr. Haluk DARENDELİLER

December 2004, 77 pages

Friction is one of the important parameters in metal forming processes since it affects metal flow in the die, forming load, strain distribution, tool and die life, surface quality of the product etc. The range of coefficient of friction in different metal forming applications is not well known and the factors affecting variation are ambiguous. Commercially available FEA packages input the coefficient of friction as constant among the whole process which is not a realistic approach.

In this study, utility of user-subroutines is integrated into MSC SuperForm v.2004 and MSC Marc v.2003 FEA packages, to apply a variable coefficient of friction depending on the contact interface conditions. Instead of using comparatively simple friction models such as Coulomb, Shear (constant) models, friction models proposed by Wanheim-Bay and Levanov were used to simulate some cold forging operations. The FEA results are compared with the experimental results available in literature for cylinder upsetting. Results show that, large variation on the coefficient of friction is possible depending on the friction model used, the part geometry and the ratio of contact normal pressure to equivalent yield stress. For the ratio of contact normal pressure to equivalent yield

stress values above 4, coefficient of friction values are approximately same for both friction models.

Keywords: Friction in Metal Forming, Finite Element Analysis, General Friction Model, Cold Forging

ÖZ

SOĞUK DÖVME İŞLEMİNDE SÜRTÜNME ANALİZİ

CORA, Ömer Necati
Yüksek Lisans, Makine Mühendisliği Bölümü
Tez Yöneticisi: Prof. Dr. Metin AKKÖK
Ortak Tez Yöneticisi: Prof. Dr. Haluk DARENDELİLER

Aralık 2004, 77 sayfa

Kalıp içindeki metal akışı, şekillendirme kuvveti, şekil değişimi dağılımı, takım ve kalıp ömrü, yüzey kalitesi gibi parametreleri etkilediği için sürtünme; metal şekillendirme işlemlerindeki önemli parametrelerden biridir. Farklı metal şekillendirme işlemleri için sürtünme katsayısı aralığı çok iyi bilinmemektedir ve sürtünme değişimini etkileyen faktörler belirsizdir. Ticari sonlu elemanlar analiz programları sürtünme katsayısını gerçekci olmayan bir yaklaşımla tüm işlem boyunca sabit olarak alırlar. Bu çalışmada, temas arayüzündeki durumlara bağlı olarak değişen bir sürtünme katsayısı uygulayabilmek için, kullanıcı tarafından yazılan programcıklar, MSC SuperForm v.2004 ve MSC. Marc v.2003 sonlu eleman analiz programlarıyla bütünleştirilmiştir. Göreceli olarak basit olan Coulomb, Kayma (sabit) sürtünme modelleri yerine; Wanheim-Bay ve Levanov tarafından önerilen sürtünme modelleri bazı soğuk dövme işlemlerinin benzetiminde kullanılmıştır. Sonlu eleman analiz sonuçları, silindir basma işleminin literatürde bulunan deneysel sonuçları ile karşılaştırılmıştır.

Sonuçlar, kullanılan sürtünme modeline, parça geometrisine ve temas basıncının eşdeğer akma gerilmesi oranına bağlı olarak; sürtünme katsayısında büyük bir değişimin mümkün olabileceğini göstermiştir. Temas

basıncının eşdeğer akma gerilmesi oranına oranının 4.0 değerinden büyük olması durumunda, sürtünme katsayısı, iki model için de yaklaşık olarak aynıdır.

Anahtar Kelimeler: Metal Şekillendirmede Sürtünme, Sonlu Elemanlar Analizi, Genel Sürtünme Modeli, Soğuk Dövme

To the memory of my paternal grandmother H. CORA……..

ACKNOWLEDGEMENTS

At first I would like to express my gratitude to my thesis supervisor and co-supervisors Prof. Dr. Metin AKKÖK, Prof. Dr. Haluk DARENDELİLER and also to Prof. Dr. Mustafa İlhan GÖKLER for giving me the opportunity to prepare this thesis, and their continuous help, encouragement, valuable discussions, guidance and patience.

I would like also to thank to Mechanical Engineering Department of Middle East Technical University and Scientific Human Resources Development Program (ÖYP), where I had been a teaching assistant there throughout this study, for giving me invaluable knowledge at the starting point of my academic career.

My sincere thanks go to my friends at Metal Forming Group for their co-operations, and to precious engineers from BİAS and TEKNOTASARIM for their help in my software related problems.

Finally; I wish to express my sincere thanks to my family for their infinite support and to my friends who encouraged and assured me continuously along this study.

TABLE OF CONTENTS

CHAPTERS

LIST OF TABLES

LIST OF FIGURES

LIST OF SYMBOLS

τ :	Friction (Shear) Stress
q:	Local Normal (Contact) Pressure
μ :	(Coulomb) Coefficient of Friction
f:	Friction factor
α:	Ratio of Real Contact Area to the Apparent Area
k:	Shear Flow Stress (Yield stress in pure shear)
σ_0:	Equivalent Yield Stress
i:	Interfacial Shear Strength Ratio(=Normalized friction stress=$\frac{\tau}{k}$)
π_C :	Power Consumption
S_C:	Contact Interface
U_r:	Relative Velocity
τ_n :	Friction Shear Stress between material and die
U_0:	An Arbitrary Constant much smaller than the relative velocity
$\bar{\sigma}$:	Effective Stress
$\dot{\bar{\varepsilon}}$:	Effective strain rate
T_i :	Surface Traction
K:	Sufficiently Large Positive Constant
$\dot{\varepsilon}_V$:	Volumetric Strain Rate Component
V:	Control Volume

CHAPTER I

INTRODUCTION

In this chapter, a brief description of friction, early studies on it, its importance in forming processes are given, and definition of metal forming and forging, new concepts in metal forming will be reviewed.

1.1 Definition of Metal Forming:

Metal forming, according to DIN 8580, is manufacturing by plastic (permanent) change of the form a solid body by preserving both the mass and the cohesion. Metal forming processes can be categorized into several groups such as with respect to forming mechanism (tensile, compressive, bending effect, by shearing), part to be formed (bulk, sheet), time-dependency (time-independent and dependent processes such as extrusion and upsetting), or forming temperature (cold, warm, hot forming). Hot forming has advantages of softening and recrystallization to make metal easier to form, while in cold forming raising the strength of the product by strain hardening is possible. Cold forming may also permit higher geometric accuracy and surface finish by avoiding thermal problems such as oxidation and distortion.

1.1.1. Forging

Forging is one of the most popular production techniques that it can be used for mass production as well as the production of individual sample parts. It was used for producing the high quality swords and hammering of gold foil, between a rock, the anvil, and a stone, the hammer in ancient times. Afterward, as the technology

advanced forging is used to produce cannon and rifle parts. Today, forging is used in different industries for the manufacturing of variety parts such as; balls for rolling bearings, small bolts, pins as well as gears, cam and crankshafts, shafts, axles, holding hooks, flanges, hand tools aircraft landing structures, turbine blades, some medical instrument components such as surgery blades etc. As in metal forming there are different classifications for forging such as in terms of temperature (hot, isothermal, warm and cold forging), die (open, closed-die), shape (compact shapes, disk shapes, long shapes)

Cold forging is a process that the bulk workpiece is placed between die and punch and subjected to compressive load. Forming temperature is room temperature and the process is a time-dependent process. Parts manufactured with the cold forming have better surface quality, and higher geometric accuracy, fatigue strength, ductility and improved grain structure.

1.2 Definition of Friction

Friction, in a simple manner, can be described as "surface resistance to the relative sliding or rolling motion" while in metal forming operations this term converts to "workpiece-die surface resistance to metal flow".

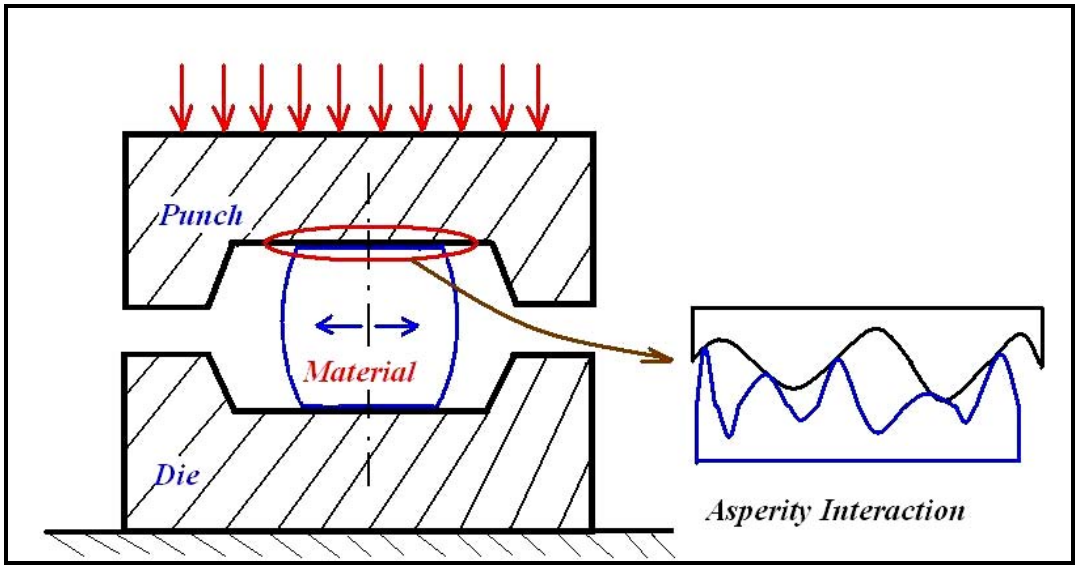

Figure 1.1 Surface Asperity Interaction between Die and Workpiece

On the contrary to its simple definition, friction is very complex phenomenon in metal forming and includes several parameters that interact with one another such as; sliding speed, contact pressure, surface roughness, material properties, temperature, lubrication condition.

1.2.1 History of Friction

Early studies related with friction go back to 15th century. **Leonardo Da Vinci** (1452-1519) was one of the scholars studied friction systematically. All types of friction were the focused subjects and differences between sliding and rolling friction were determined. Da Vinci stated the two basic laws of friction as follows:

1. The areas in contact have no effect on friction.
2. If the load of an object is doubled, its friction will also be doubled.

Amontons (1663-1705) rediscovered the two basic laws of friction that had been discovered by Leonardo Da Vinci. Amontons concluded an experimental work which was on friction of unlubricated solids and published it in 1699. Main outcome was that "Frictional force is independent of the areas in contact and directly proportional to the normal load. It was also found that the frictional force was always equal to the one-third of normal load.

The most systematic research on friction was done by **Coulomb** (1736-1806). The influence of a large number of variables on friction was investigated and added to the second law of friction, " Strength due to friction is proportional to compressive load and it's independent of sliding velocity" , "although for large bodies friction does not follow exactly this law". Coulomb published the work referring to Amontons. The second law of friction is known as the "Amontons-Coulomb Law" referring to work done by the two scientists in 1699 and 1785 respectively.

In 20th century; **Bowden and Tabor** (1950) gave a physical explanation for the law of friction which is known "Adhesion Theory". Theory states that the true area of contact is a very small percentage of the apparent contact area and it is still valid today. The true contact area is formed by the asperities. As the normal force increases, more asperities come into contact and the average area of each asperity contact grows. The frictional force was shown to be dependent on the true contact area—a much more intuitively satisfying argument than what the Amontons-Coulomb law allows [1].

Studies on friction have been varied and detailed in past few decades. Different friction models have been proposed for different applications and the researches are going on uninterruptedly. Technological developments such as SFM (Scanning Force Microscope) and SFFM (Scanning Force and Friction Microscope) not only provide the opportunity to investigate the friction on microscopic scale but also make easy these researches [2].

1.2 Importance of Friction in Metal Forming

In metal forming operations; friction has great importance since affects the forming force (or energy), material flow inside the die, and as result of these product quality and tool life. In addition to operations, in finite element simulations; friction model is one of the key input boundary conditions. Among the various friction models in literature which one is of higher accuracy is still unknown and controversial [3]. It is also difficult to establish a unique friction model that includes all forming parameters for all metal forming operations. In commercial Finite Element Analysis (FEA) packages there are different friction models such as Coulomb, Shear, Stick-Slip models. However, these models are incapable to simulate the friction accurately. Furthermore they use constant coefficient of friction during the whole process which is not realistic. Although coefficient of friction values for

metal forming operations are known for different applications; the changing characteristics of it is ambiguous.

Table 1.1 Friction Coefficients for Forming Operations [4]

	Coefficient of Friction μ	
Process	**Cold**	**Hot**
Rolling	*0.05-0.1*	*0.2-0.7*
Forging	*0.05-0.1*	*0.1-0.2*
Drawing	*0.03-0.1*	___
Sheet-metal forming	*0.05-0.1*	*0.1-0.2*
Machining	*0.5-2*	___

1.4 Scope of This Study

The outline of the thesis is as follows:

Chapter I give information about fundamental definitions.

In Chapter II, the friction theories and friction models in bulk metal forming are introduced. This chapter also includes the review of ring compression test.

Chapter III deals with the theory and finite element formulation.

Case studies related to the analysis of friction in cold forging operations are given in Chapter IV.

Finally, Chapter V is devoted to the conclusions and suggested future works.

CHAPTER II

THEORIES OF FRICTION AND FRICTION MODELS

This chapter includes early theories for friction, a short review to friction models in sheet metal forming, and the most eminent friction models in bulk metal forming and related literature surveys, differences and similarities between those. Finally, a general conclusion for friction models and information on friction tests were presented.

2.1 Theories of Friction

In order to analyze or to simulate the contacted surfaces accurately tribologists have been studying on effects of lubrication, wear and friction. The earlier theory for the friction is known as *roughness theory* which is not good explanation for friction in engineering.

$$\mu = \frac{F}{N} = \tan\theta \tag{2.1}$$

The theory accepts that one of the surfaces in contact is much harder than the other and the angle between asperities is between 5-10 degrees. This theory is also named as non-dissipated theory.

Plowing (or ploughing) theory considers a hard cone moving ahead in a softer material. When the cone, move forward in the softer material; fully plastic deformation occurs. According to this theory; friction value is independent from load, velocity of cone, and it's only depended on cone angle.

$$f_p = \frac{2\tan\theta}{\pi} \qquad (2.2)$$

Bowden and Tabor can be considered as the pioneers of modern tribologists. They proposed [5] *adhesion theory* to describe the friction which is still commonly accepted theory today although it's been modified. Different from the above two models adhesion theory does not include the geometric parameters.

$$f_a = \frac{F}{N} = \frac{\tau}{H} = \frac{S_{sy}}{H} \cong \frac{1}{6} \simeq 0{,}18\ ; \qquad (2.3)$$

Where τ : Shear Stress , H: Hardness ,

S_{sy} : Yield Strength of the Weaker Material which Fails due to Shearing

This theory is stated as "Two clean and dry surfaces, regardless of smoothness of their surfaces, contact each other at only a fraction of their apparent area of contact. In such a condition, the normal load is supported by the asperities. Due to the high stresses on asperities; plastic deformation occurs at the junctions. As a result of this asperities form microweld (Figure 2.1).

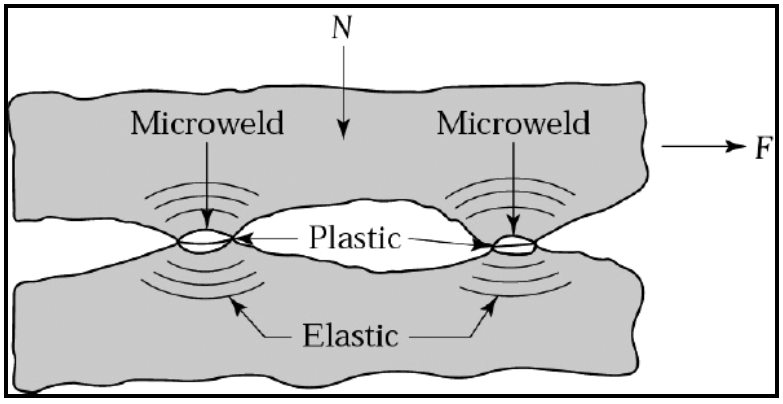

Figure 2.1 Asperities on the two bodies which are in contact [4]

However adhesion theory can not explain the different friction values. To overcome the deficiencies; modified adhesion theory was developed. In this new approach

failure theory for the 3-D stress elements used. Junction growth is also taken into account during the sliding.

2.2 A Glance to Friction Models in Metal Forming

Friction models in metal forming can be categorized in to two groups:

1) Friction Models for Sheet Metal Forming
2) Friction Models for Bulk Forming

In sheet metal forming; modeling friction is more complex than the one in bulk forming. Wilson [6] has pointed out that relatively simple friction models such as Amontons-Coulomb can not reflect the, influence of process variables on friction. This greatly limits the usefulness of simulation as a design tool. In earlier studies of Wilson friction models for tool-workpiece friction in metal forming processes operating in the boundary lubrication regime were developed. Then; the friction model for sheet metal forming applications can be operated on both mixed and boundary lubrication was established [7]. Wilson also pointed out the importance of pressure, sliding velocity, lubrication condition and surface roughness on friction. Flow chart for Wilson's Friction Model for different film thicknesses is given in Figure 2.2.

Integrating Wilson's friction model into a finite element program, Darendeliler, Akkök, and Yücesoy [8] analyzed sheet metal forming processes with the variable coefficient of friction. In another study; Polycarpou and Soom [9], [10], [11] developed two-dimensional dynamic friction models at a lubricated line contact, operating in boundary and mixed lubrication regimes. It is stated that the friction model includes the sliding velocity and the instantaneous separation of the sliding bodies, normal to the sliding direction, the normal load and fluid properties. For a clearer physical interpretation of friction coefficient; it is separated into two components as fluid shear and solid components [12].

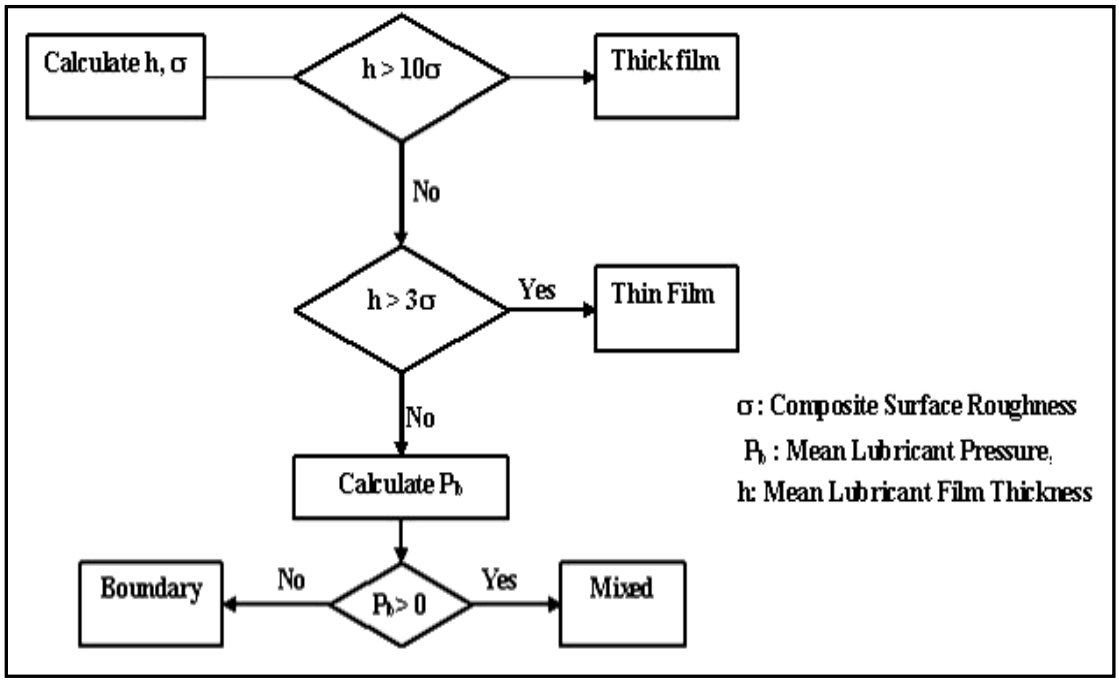

Figure 2.2 Flowchart for Wilson's friction model

2.2.1 Amontons-Coulomb (or Da Vinci) Model

Friction is most commonly characterized by using constant coefficient of friction model variously attributed to Amontons, Coulomb, or Da Vinci.

$$\tau = \mu.q \tag{2.4}$$

τ : Frictional Stress

q: Local Normal Pressure

μ : (Coulomb) Coefficient of Friction

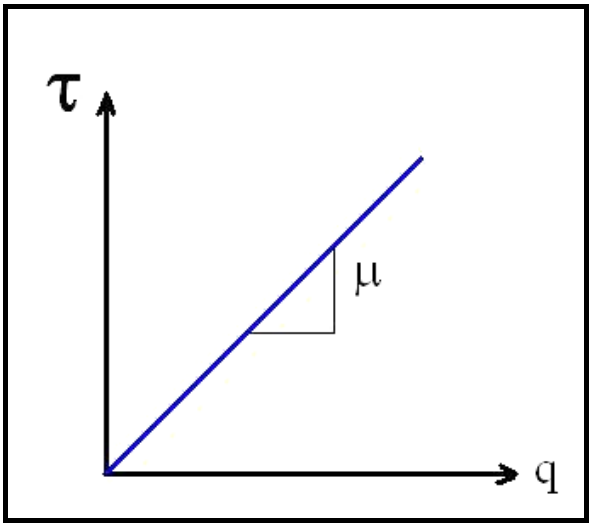

Figure 2.3 Coulomb-Amontons friction model

Dry slipping occurs over the whole tool/workpiece interface. Friction stress τ is directly proportional to local normal pressure q. It is used for most applications due to its simplicity.

2.2.2 Constant Friction Model

This model proposed by Orowan in 1943. Model assumes that; friction stress is proportional to interface pressure –as in Amonton-Coulomb Model- until a critical value of interface pressure is reached. Above the critical pressure, which is associated with real area of contact becoming equal to the apparent area, the friction stress is constant and equal to yield stress in pure shear k. It is the one of most popular models since its simplicity and seemingly indicating the material feature of plastic deformation. However; it is not accurate since friction does not depend on the current state of stress at the tool-workpiece interface, but simply on material property.

$$\tau = m.k \tag{2.5}$$

Where

τ : Frictional Stress

m: Friction factor

k: Shear flow stress

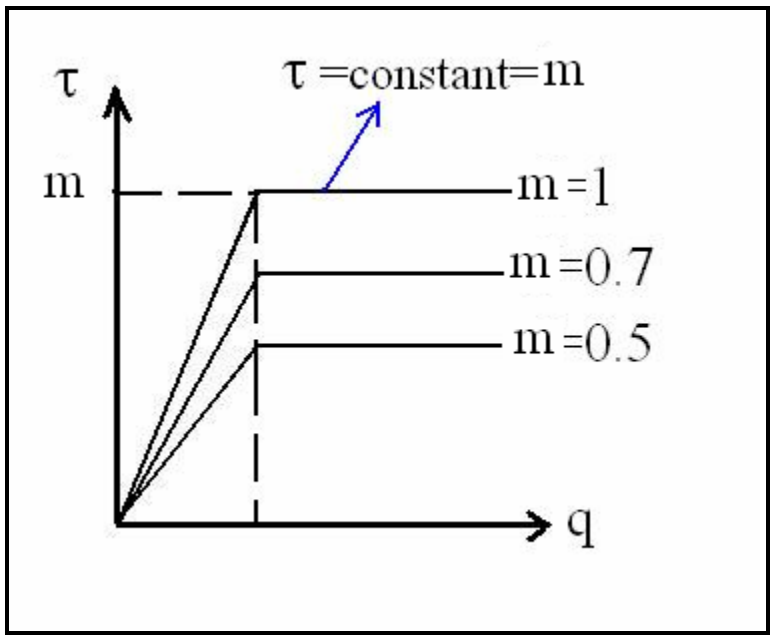

Figure 2.4 Constant Friction Model

Friction models, mentioned up to here, are relatively insufficient to model bulk metal forming operations since those are simply depend on either material property or normal pressure value.

2.2.3 General Friction Model

In an earlier study; Wanheim [13] stated that Amonton's friction law should not be applied when the normal pressure is higher than approximately yield stress of the material. It was also put forward the necessity of considering the frictional stress as a function of normal pressure, surface topography, length of sliding, viscosity, and compressibility of the lubricant. With this aim Wanheim, Bay, and Petersen

developed a general friction model [14]. The model can be considered as an updated model of constant friction. Theory is based upon the slip-line theory as a model of analysis.

$$\tau = f \cdot \alpha \cdot k \tag{2.6}$$

Where

τ : Friction Stress

f**:** Friction factor ($0 \leq f \leq 1$)

α: Ratio of real contact to the apparent contact area

k: Shear flow stress (Yield stress in pure shear)

The real contact ratio α and frictional stress τ are determined as functions of the nominal normal pressure $\frac{q}{\sigma_0}$ and the friction factor f is given in Figure 2.4.

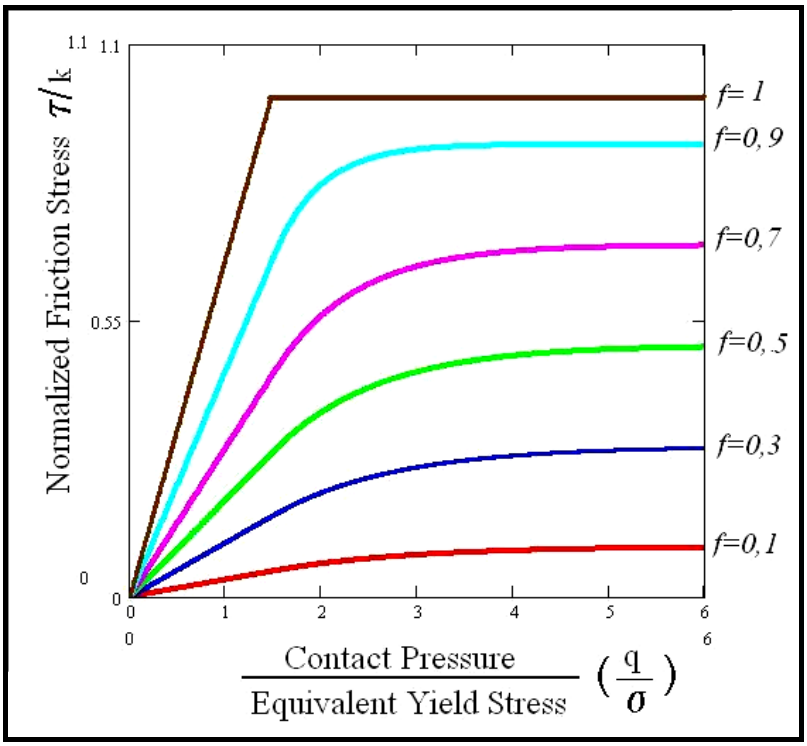

Figure 2.5 Normalized friction stress as a function of nominal normal pressure and friction factor for the General friction model.

The model assumes that the friction to be proportional to the normal stress at low normal pressure ($\frac{q}{\sigma_0} < 1.5$), but going towards a constant value at high normal pressure ($\frac{q}{\sigma_0} > 3$). These two ranges are being combined by the intermediate transition region as shown in Figure 2.4.

In practice the friction factor f is determined experimentally;

$$f = \cos 2\theta \tag{2.7}$$

Where, θ is the angle between β slip-lines and the tool-specimen interface. The term α is given by the analytical expressions of Wanheim-Bay friction model developed by Gerved[15]:

$$(f \cdot \alpha =) \frac{\tau}{k} = \frac{q/\sigma_0}{q'/\sigma_0} \cdot \frac{\tau'}{k} \qquad (\text{For } q \le q') \tag{2.8}$$

$$(f \cdot \alpha =) \frac{\tau}{k} = \frac{\tau'}{k} + \left(f - \frac{\tau'}{k}\right) \cdot \left(1 - \exp\left[\frac{\frac{\tau'}{k}\left(\frac{q'}{\sigma_0} - \frac{q}{\sigma_0}\right)}{\frac{q'}{\sigma_0}\left(f - \frac{\tau'}{k}\right)}\right]\right) \qquad (\text{For } q > q') \tag{2.9}$$

Where the limit of proportionality $\left(\frac{\tau'}{k}, \frac{q'}{k}\right)$ is given by:

$$\frac{q'}{\sigma_0} = \frac{1 + \frac{\pi}{2} + \arccos(f) + \sqrt{1 - f^2}}{\sqrt{3}\left(1 + \sqrt{1 - f}\right)} \tag{2.10}$$

$$\frac{\tau'}{k} = 1 - \sqrt{1-f} \tag{2.11}$$

It was found that friction conditions at high normal pressures differ very greatly from friction conditions at low normal pressures. Amonton's law is valid only until $\frac{q}{\sigma_0} = 1.3$ irrespective of friction factor value. Starting from this point, coefficient of friction would become pressure dependent. In metal working processes normal pressure is often considerably greater than the yield stress of the material and consequently in Amonton-Coulomb's law friction stress becomes greater than yield stress of the material in pure shear. However, Amonton's law in the case of small f values (f<0.2) is nearly correct at high pressures [14].

2.2.4 Torrance's Friction Model

Based on Slip line theory; Torrance[16] assumed that an asperity contact can be represented as a hard wedge which slides over a soft ductile surface, pushing a plastic wave ahead of it as shown in Figure 2.6.

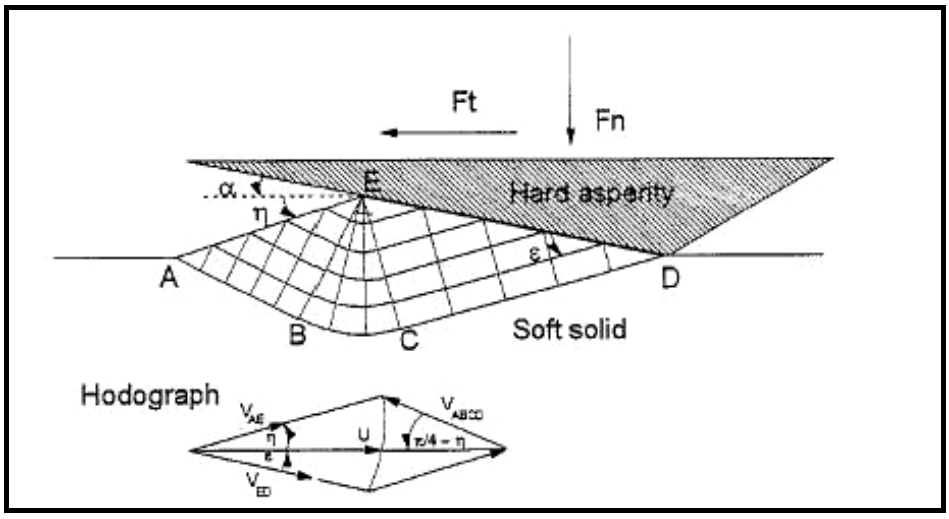

Figure 2.6 Slip line field model of asperity interaction

To predict the stress and strain in the softer material slip line fields can be developed. Both stress and strain are depend on the interfacial shear strength ratio (or normalized fiction stress), as used in Bowden and Tabor's theory. Using following equations; coefficient of friction can be determined:

$$F_T = \left[A.\sin\alpha + \cos(2\varepsilon - \alpha)\right] \cdot \overline{EDk} \tag{2.12}$$

$$\mathrm{F_n} = \left[A.\cos\alpha + \sin(2\varepsilon - \alpha)\right] \cdot \overline{EDk} \tag{2.13}$$

$$\mu = \frac{F_T}{F_n} \tag{2.14}$$

Where F_T and F_n are the traction and the normal forces per unit width of wedge; while k is the shear yield strength of the softer material and

$$A = 1 + \frac{\pi}{2} + 2\varepsilon - 2\eta - 2\alpha \quad , \quad 2\varepsilon = \arccos(i) \text{ and } \quad \mathrm{i} = \frac{\tau}{\mathrm{k}} \tag{2.15}$$

It is stated that provided the asperity contacts are mainly plastic, the above model gives a reasonable account of the effects of changing surface texture on μ in single asperity tests and for real surfaces. Experimental results show also well agreement with finite element calculations.

Main conclusion for Torrance's model is that coefficient of friction should fall with surface slope, and with interfacial shear strength. This model is not suitable all metal forming operations and doesn't permit to use coefficient of friction as variable.

2.2.5 Levanov's Friction Model

Equation 2.16 represents the friction model of FORM2D (Finite Element System for Simulation and Analysis of Forming Process Quantor Ltd. Moscow 1996) proposed by Levanov [17] and it was investigated by Hallström [18].

$$\frac{\tau}{k} = f\left[1 - \exp\left(-1.25\left(\frac{q}{\sigma_0}\right)\right)\right] \tag{2.16}$$

It is the special case of more general empirical model presented by Stephenson [19] and in agreement with the General Friction Model proposed by Wanheim et al. [14]. Both models deal with the non-linear friction forces and are based on the relation of real contact area and apparent area. Figure 2.7 shows the Levanov's model for different friction factors while Figure 2.8 represents both Levanov's and General Friction Model for same friction factors.

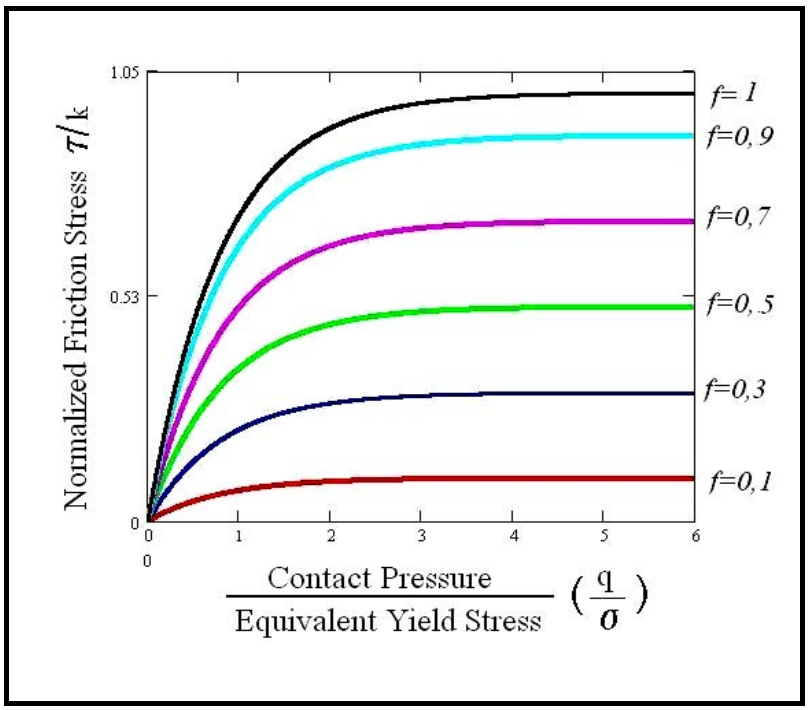

Figure 2.7 Levanov's friction model

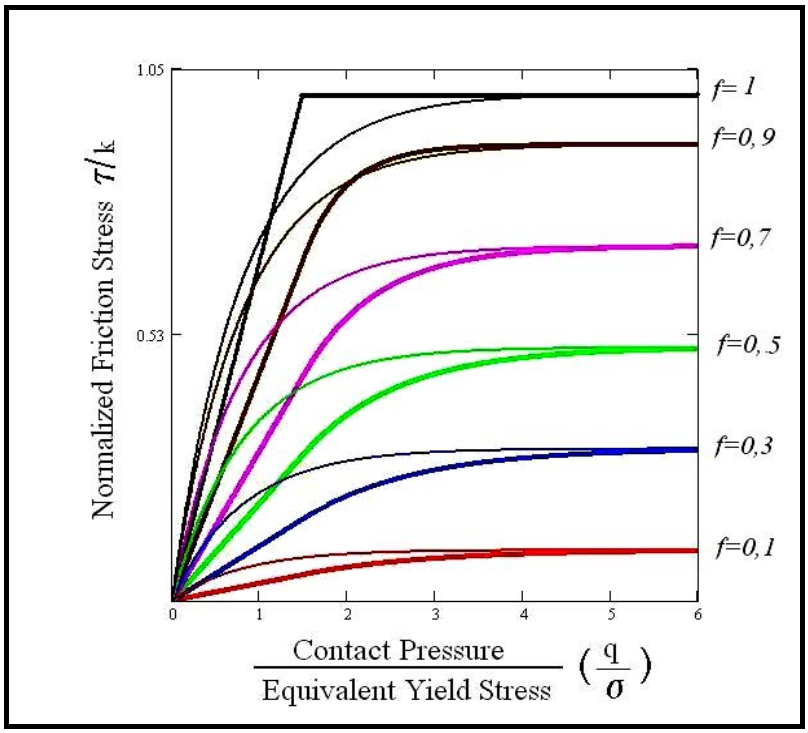

Figure 2.8 Comparison of Levanov's and Bay's friction models

(thinner ones are for Bay's Model)

Hallström used Levanov's friction model in order to find the best average friction factor on the tool-workpiece interface to obtain the most realistic filling when simulating material flow in counterblow hammer forging [18].

Although it is not used widely and Hallström stated that some concurrent results for counterblow hammer forging had been found. As a conclusion, it is clear that Levanov's model is more efficient than the conventional friction models in simulating friction.

2.3 General Evaluation of Friction Models

There are lots of friction models given in literature. The models mentioned above are the eminent ones in bulk metal forming.

One can say that with the new models taking into account the non-linear frictional forces and asperity deformation during the process have advantages in analyzing friction. For example, researches showed that using general friction model better estimation of the material flow than Amonton's law are obtained. [14] Same conclusion can be given for Levanov's Model which is similar to General Friction Model. Even tough the validity of the General Friction Model had verified experimentally, its implementation in FE software for metal forming has so far been limited. Studies were limited to small stages of deformation. Therefore this model also must be verified with other bulk metal forming operations.

A comprehensive research made by Tan [3] investigating differences between five friction models (including Coulomb's, Constant and General friction models and two others) in obtaining friction calibration curves showed that there is no definite difference between these models and they do well agreement with the FEA, although they are very dissimilar.

The most important conclusion for friction models is that it is difficult to establish a friction model that valid for all kind of metalworking processes for different conditions. With the better understanding and analyzing of friction it will be possible to understand the metal flow, forming loads inside a die accurately and it leads to reduce the number of die design trial-error processes.

Studies both theoretical and experimental have been carried out continuously to get better friction modeling have great importance since it is being one of the key inputs in Finite Element Analysis. International collaborations and competitions will provide more knowledge about friction phenomena. A research project can be given as an example to those collaborations, supported by EU, aims to develop 3-D finite element code for forging. [20]

2.4 Ring Compression Test

The ring-compression test is an experimental method used for the determination of frictional conditions in bulk metal forming. It is initially proposed by Kunogi in 1956 then developed by Male and Cockroft in 1964-65 [21]. It provides quantitative evaluation of friction and gained wide acceptance around the world. The concept of the test is the increasing or decreasing of the inner diameter of a short ring specimen when it is compressed between two flat, parallel platens. It provides a particular knowledge about the coefficient of friction at the workpiece-die interface. If the friction is low (good lubrication) the internal diameter increases; while if the friction is high (poor lubrication) the internal diameter is decreases as shown in Figure 2.9. Figure 2.10 shows an example to the increased internal diameter.

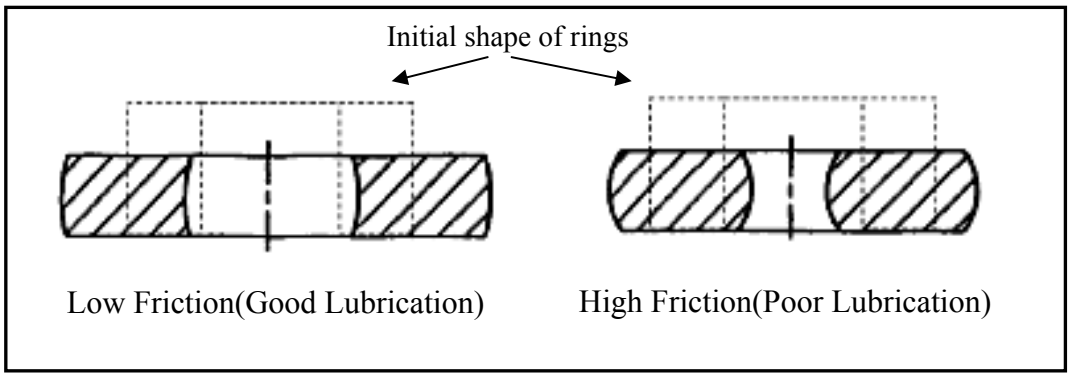

Figure 2.9 Two possible results for ring compression test

Figure 2.10 Test result for ring compression [22]

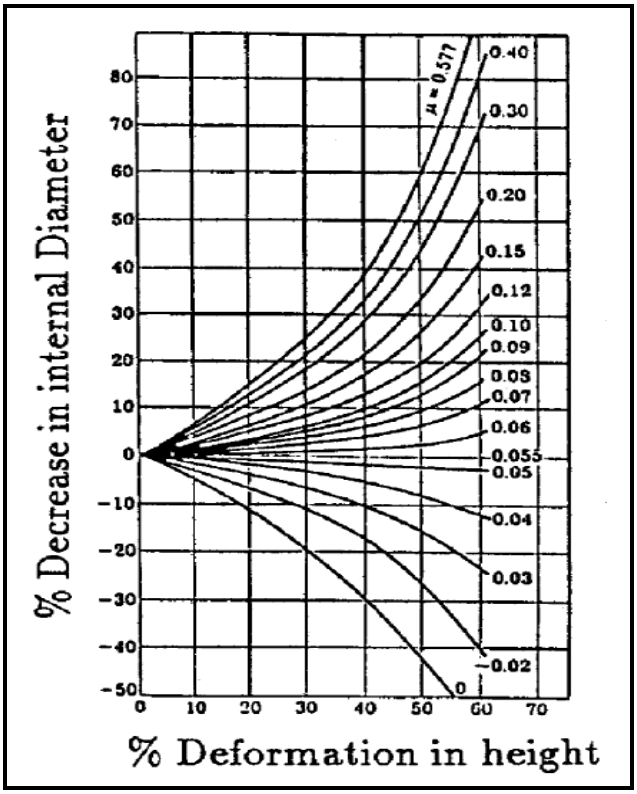

Figure 2.11 Friction calibration curves obtained from the ring compression test in terms of μ [23]

Calibration curves are formed to ring geometries. Each ring geometry; has its own specific set of curves. The most common ring geometry is 6:3:2 where the first number denotes the outer diameter; and the second number denotes the internal diameter while the last one is for height of the ring.

The actual size of the specimen is usually not relevant in these tests. Thus once the percentage of reduction in internal diameter and height are known, one can determine coefficient of the friction using the appropriate chart.

The major advantages of the ring-compression test are that it does not require any force measurement and that it involves large-scale deformation of the workpiece material, as is the case in actual practice. This test can also be used to rate different metalworking fluids.

There are some modified models of ring compression test. Petersen et al. developed new ring test geometry that it allows the characterization of friction under

low pressure conditions [24]. An alternative method which is named "open-die backward extrusion test technique" was developed to quantitatively evaluate the coefficient of friction μ at the tool-workpiece interface [25]. This technique relates the percentage deformation in height of the specimen to the percentage increase in extruded height of the specimen.

2.5 Double Cup Extrusion Test

Developed by Geiger, this test eliminates the backwards of ring compression test in high interface pressures and severe deformation. The test combines the single cup forward and single cup backward extrusion which reflects the real process conditions more accurately. Figure 2.12 shows the principle of test where, h_1 is the upper cup height, h_2 is the lower cup height. The cups were generated by the simultaneous action of punches inside a cylindrical container. In the test lower die is stationary while the upper die travels downward.

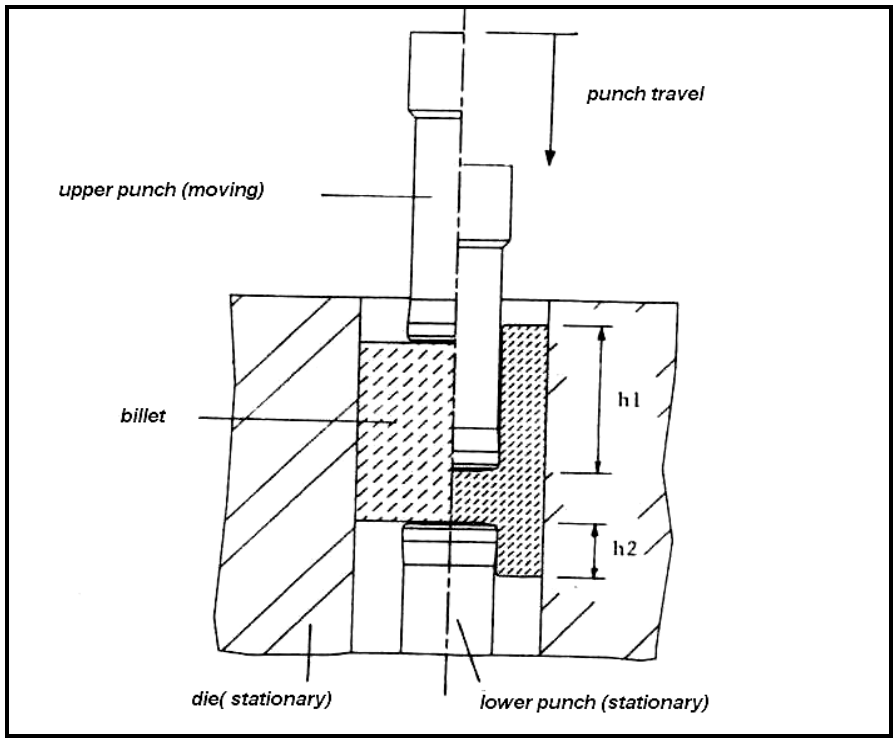

Figure 2.12 Principle of double cup extrusion test [26]

Output of Double-Cup Extrusion Test (DCET) is the cup heights and those are used to determine cup height ratio as follows:

$$R_{CH} = \frac{h_1}{h_2}$$

Fundamental knowledge about DCET is cup height ratio increases with the increasing coefficient of friction and if the friction is very low, the two cups will have same height while in severe frictional conditions, the forward extrusion cup will be prevented.

DCET used for ranking the lubricants based on the above cup height ratio. Moreover, using this technique surface analysis can be done on cut specimen to investigate galling. Figure 2.13 shows an experiment sample.

Figure 2.13 Double cup extrusion test result [27]

Forcellese et. al. [28] stated that the double cup extrusion test is strongly influenced by the friction shear factor and the loads required for the double cup extrusion are lower than the ones needed for single forward and backward extrusions.

CHAPTER III

THEORY AND FINITE ELEMENT FORMULATION

Chapter III is devoted to theory and analysis of finite element, friction modeling in FEA, finite element types used in the analysis, modeling friction in FEA, and user subroutine utility in MSC Marc.

The commercial Finite Element Analysis package, MSC MARC-Mentat 2003 [29], MSC Superform version 2004 [30], and Compaq Visual Fortran v. 6.6 are used in this study [31].

3.1 Steps of the Finite Element Analysis

To be able to successfully apply the finite element method to the metal forming operations the following requirements should be fulfilled [32]:

1. The physical problem should be well-defined for the application of simulation.

2. The idealization of this problem should be done correctly: Simplifications and assumptions should be reasonable. Unnecessary details should be eliminated.

3. The idealized problem should have the correct spatial discretization: Type of elements used, topology of element mesh, and the density of element mesh should be constructed according to the nature of problem.

4. Boundary conditions of the physical model should be investigated and applied in the simulation: friction, heat transfer, machines, dies etc.

5. Correct material laws and parameters should be used in the simulation: flow curve, anisotropy, failure, etc.
6. Numerical parameters used in the simulation should be chosen accordingly: penalty factors, convergence limits, increment sizes, remeshing criterion etc.

7. The simulation should be "economical": Computation times and the time required to prepare the model should be reasonable, storage requirements of the model and the results should also be within physical limits.

8. The results should be evaluated carefully and checked whether they are reasonable or not.

3.2 Linear and Nonlinear Finite Element Analysis

A problem is considered as a linear if the followings are satisfied:

1. Displacements are infinitesimally small
2. Gradients of displacements are infinitesimally small
3. Stresses depend on linearly strains
4. Boundary conditions do not change during loading

However, if the force-displacement relationship depends on the current state (current displacement, force and stress-strain relations) problem is nonlinear. Nonlinear, high-temperature behavior of materials in nuclear industry and geometric nonlinearities

such as buckling led to the development of nonlinear finite element techniques. There are three types of nonlinearity:

1. Material nonlinearity (physical)
2. Geometric nonlinearity (kinematic)
3. Changing boundary conditions

Material nonlinearity is due to the nonlinear relation between stress and strain like in elastic-plastic (elastoplastic), elasto-viscoplastic materials, creep, composite and concrete structure problems etc. Geometric nonlinearity is aroused from nonlinear relationship between strains and displacements, and nonlinear relationship between stresses and forces. Large strain problems such as manufacturing, impact and crash can be given as examples to this type of nonlinearity. Changing boundary conditions also contribute to nonlinearity. If the loads on the structure vary with the displacements nonlinearity occurs. Moreover contact and friction problems lead to nonlinear boundary conditions. Most of the metal forming applications can be given as examples.

3.3 Finite Element Formulations

There are two fundamental approaches in the finite element method. These are Lagrangian and Eulerian formulations. Eulerian formulation is generally used in fluid mechanics applications. In solid mechanics, Lagrangian meshes are used widely because it is possible to handle complicated boundaries and follow material points, so that history dependent materials can be treated accurately.

In this study updated Lagrange formulation was used.

3.4 Finite Element Types Used in Analyses

Different types of elements used in analyses. Due to axisymmetry of the problem in Case Study I, element type 10 is used (Figure 3.1). It is a four-node, isoparametric, arbitrary quadrilateral written for axisymmetric applications. As this element uses bilinear interpolation functions, the strains tend to be constant throughout the element. This results in a poor representation of shear behavior.

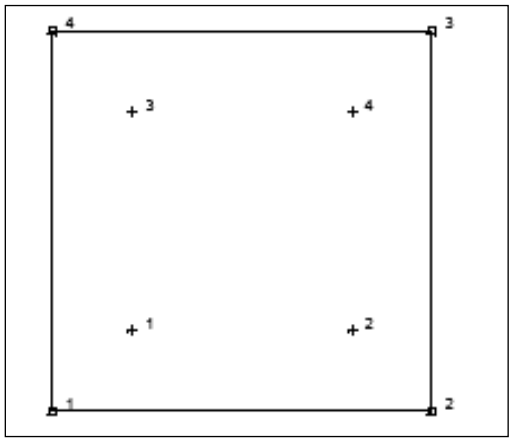

Figure 3.1 Integration points for element type 10

This element is preferred over higher-order elements when used in a contact analysis [33].

To reduce the number of integration points, consequently computational time, triangular elements should be used. In this case element type 2 is preferred (Figure 3.2). It is a three-node, isoparametric, triangular element. It is written for axisymmetric applications and uses bilinear interpolation functions. The strains are constant throughout the element and this results in a poor representation of shear behavior.

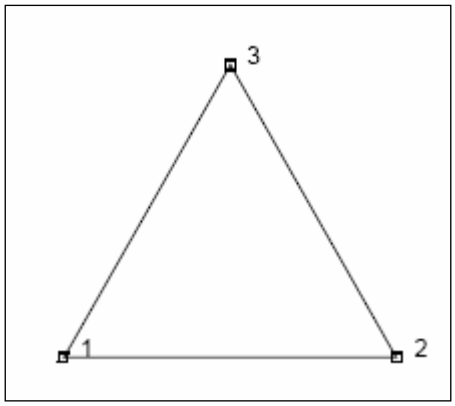

Figure 3.2 Integration points for element type 2

3.5 Friction Modeling in Finite Element Analysis

In bulk metal-forming analysis constant friction model is used extensively. In terms of finite-element programming; implementation of friction model can be done in two different ways: Some analysts utilize a very thin layer of elements at the boundary, with the die sides nodes fixed and having material behavior such that shear yield stress is a certain factor of the hydrostatic pressure of the deforming material in contact with the layer, whilst others specify the frictional stress at the tool-workpiece interface as a traction boundary condition. The popularity of first technique is attributable not to its accuracy but to its simplicity.

Assuming friction to be a traction boundary condition, the power consumption π_C, due to friction can be expressed by:

$$\pi_C = \int_{S_C} \int_0^{U_r} (\tau_n . dU_r) dS \tag{3.1}$$

Where, Sc is the contact interface, U_r is the relative velocity and τ_n is the friction stress between material and die. The sense of the friction shear stress is opposed to the relative velocity, U_r, according to:

$$\tau_n = -m.k.\frac{U_r}{|U_r|} \tag{3.2}$$

In order to avoid numerical problem in Equation 3.1 due to abrupt changes in the friction shear stress at the neutral point, Chen and Kobayashi proposed an alternative form for Equation 3.2, substituting the step function by an arc tangent as close to the step as desired:

$$\tau_n = mk\left\{\frac{2}{\pi}\arctan\frac{|U_r|}{U_0}\right\}\frac{U_r}{|U_r|} \tag{3.3}$$

Where, U_0 is an arbitrary constant much smaller than the relative velocity. Equation (3.3) gives a smooth transition of the frictional stress near the neutral point.

Implementation of the General Friction Model as a traction boundary condition at the contact interface calls for a modification of Equation 3.3 so that:

$$\tau_n = f.\alpha.k\left\{\frac{2}{\pi}\arctan\left(\frac{|U_r|}{U_0}\right)\right\}\frac{U_r}{|U_r|} \tag{3.4}$$

Where, f is the friction factor according to the Manheim-Bay model, and α is the ratio between the real and the apparent contact area between smooth tool and a rough workpiece surface.

After getting the power consumption due to friction term it can be inserted to the rigid-plastic FEM formulation as follows:

$$\prod = \int_V \bar{\sigma}.\dot{\bar{\varepsilon}}.dV + \int_V \frac{1}{2}K.\dot{\varepsilon}_v^{\,2}.dV + \int_{S_C}\left(\int_0^{|U_r|}\tau_n.dU_r\right).dS - \int_{S_F} T_i.U_i.dS \tag{3.5}$$

where $\bar{\sigma}$ is the effective stress, $\dot{\bar{\varepsilon}}$ is the effective strain rate, T_i represents the surface traction, K is a sufficiently large positive constant penalizing the volumetric strain-rate component, $\dot{\varepsilon}_v$, in order to enforce the incompressibility constraint on the kinematically-admissible velocity fields, and V is the control volume limited by the surfaces S_C and S_F, where velocity U_i and traction T_i are prescribed, respectively [15].

3.6 User Subroutine Utility in MSC Marc

In MSC.Marc, the user subroutine feature constitutes one of the real strengths of MSC.Marc, allowing you to substitute your own subroutines for several existing in MSC.Marc. This feature provides you with wide latitude for solving non-standard problems. These routines are easily inserted into MSC.Marc. When such a routine is supplied, it is simply replaced by the one which exists in MSC.Marc file using appropriate control setup [34]. In this study, instead of available friction models in MSC Marc; different friction model will be implemented to the MSC Marc utilizing related user subroutine UFRIC. UFRIC provides to define a friction coefficient as a function of the contact stress [35].

User subroutine facilities are realized with utilizing of FORTRAN compiler. Since the MSC Marc written in FORTRAN; user subroutines are activated with FORTRAN.

CHAPTER IV

CASE STUDIES ON COLD FORGING

In this chapter two case studies will be considered. The first one is on cylinder upsetting while the other is forming of a spherical head of a bolt. In first case study, to compare the FEA results with the experimental work cylinder upsetting was chosen. During the cylinder upsetting process the pressure distribution is almost uniform on the contact surface all along the process. However, in the second case study a different geometry is chosen to have a non-uniform pressure distribution along the process. Therefore, cold forming of spherical head of bolt is considered.

4.1 Case Study I: Cylinder Upsetting

In this case study variation of friction in a cylinder upsetting operation will be investigated. This case study is based on the experimental work done by Tan [3, 36] and its FEA solutions. In this experimental work, Tan used cylindrical billet which is extruded from AA-6082 type of aluminum. Figure 4.1 shows the workpiece to be upset and die configurations.

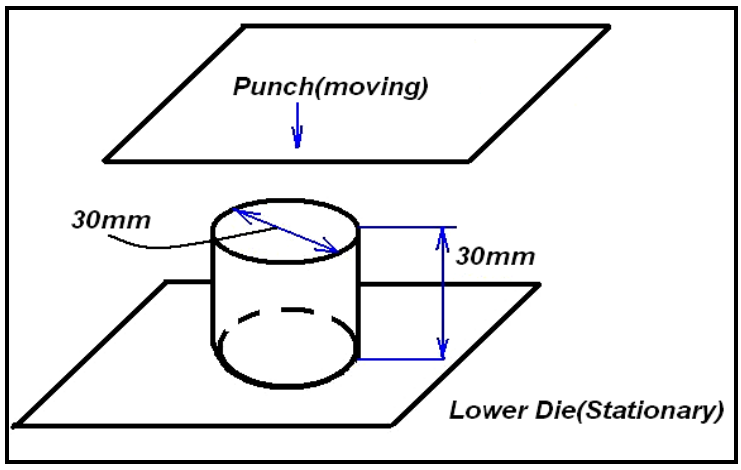

Figure 4.1 Workpiece and die configuration in cylinder upsetting

In upsetting of a cylindrical workpiece, due to friction between the flat die surfaces and workpiece barreling occurs on the free surface of the specimen. Figure 4.2 shows the upsetting of a cylinder with initial radius R_0 and height h_0 to a final height of h_1. If there is no friction at the interface there will be no bulging and the radial deformation will be uniform with a radius R_{w0} as shown in Figure 4.2.a. Using constancy of volume, the relation between the final diameter and height can be determined.

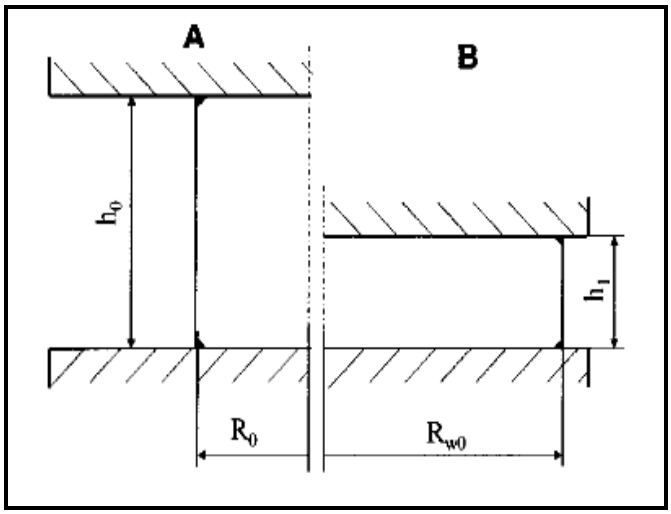

a) Contact area in upsetting without friction

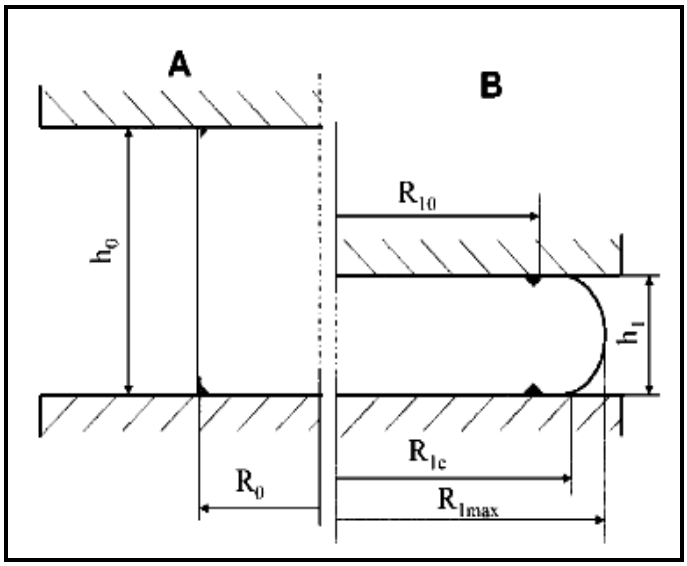

b) Contact area in upsetting with friction

Figure 4.2 Various contact areas in upsetting of cylindrical billet [36]

However in the case of upsetting with friction, radial deformation across the height of the workpiece is non-uniform and the final dimensions can not be predicted easily. Figure 4.2.b shows the expanded radius of the initial radius and the contact radius of the cylindrical workpiece.

4.1.1 Friction Area Ratio

It is well known that friction causes to immigration of material from free surface of the workpiece and this material comes into contact with the flat die surfaces. This new extra area is called as "immigrated contact area". Here, it must be emphasized that total contact area (both immigrated and expanded original contact area) obtained in the case of friction is always smaller than the area deformed without friction. To reveal the effect of friction in contact area expansion, the term Friction Area Ratio is introduced by Tan [36].

In friction area ratio, immigrated contact area is not included and determined from following equation:

$$F_r = \frac{A_{w0} - A_{10}}{A_{w0}} = 1 - \frac{h_1 \cdot R_{10}{}^2}{h_0 \cdot R_0{}^2} \qquad (4.1)$$

where

A_{w0}: Final expanded contact area deformed without friction=$\pi \cdot \mathrm{R}_{w0}{}^2 = \pi \cdot R_0{}^2 \cdot h_0 / h_1$,
A_{10} : Final expanded original contact area=$\pi \cdot \mathrm{R}_0{}^2$
R_{10} : Final radius of expanded original contact
R_0 : Original radius
h_1 : Final height
h_0 : Original height

4.1.2: Finite Element Model for Case Study I

SuperForm version 2004 and Digital Fortran v.6.6 were used in numerical simulation of the upsetting process. Due to the axisymmetric nature of problem, quarter modeling of actual workpiece is sufficient as shown in Figure 4.3. In this way both the number of elements and the solution time are reduced.

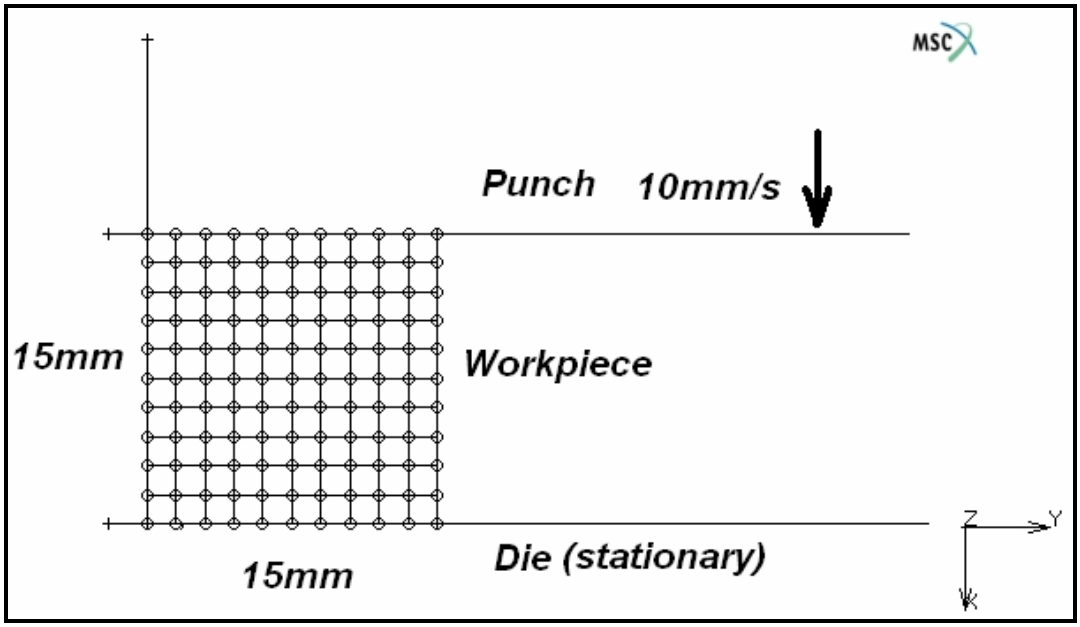

Figure 4.3 Quarter model with 100 axisymmetric quadrilateral elements

Table 4.1 summarizes the parameters used in the finite element analysis. During the analysis, the quarter workpiece model compressed from a height 15mm to 5mm, resulting in 67 % height reduction. For the determination of friction area ratio, R_{10} values are determined by using the particle tracking utility of the software. Particle tracking enables user to get positions of nodes even in remeshing during the analysis. Particle tracking data is given as a separate output file. R_{10} value, given in Figure 4.2.b, is taken for every 5 or 10 steps during the upsetting process.

Figure 4.4 shows the material flowlines and particle positions different coefficients of friction.

Table 4.1 Parameters used in FEA of cylinder upsetting

ANNEALED & WORK-HARDENED AA-6082	**ANALYSIS OPTIONS**	FEA Program	MSC SuperForm Version 2004
		Compiler for User Subroutines	Digital Fortran v.6.6
		Material Plasticity Procedure	Elastic-Plastic
		Die Material Type	Rigid
		Punch Velocity	10 mm/s (Quarter Model), 20 mm/s(Half Model)
		Number of Steps	100
		Time per Step	0.01 s
		Iteration Method	Newton-Raphson
		Remeshing	Global remeshing, overlay quad type, depends on element distortion, angle deviation: 40˚
		Max. Element Edge Length After Remeshing	0.3 mm
		Number of Elements	Quarter model: 100-2000
			Half model: 200-3600
	CONTACT	Friction Models	Coulomb, Shear (Constant), Bay's (General), Levanov's Models
		Relative Sliding Velocity	Default (=0)
		Coefficient of Friction	Constant in Coulomb, Shear ; variable in Bay's and Levanov's
		User Subroutine	UFRIC
	MATERIAL	Model	$\sigma = 220 \cdot \varepsilon^{0.19}$ (MPa) *Annealed* $\sigma = 220(0.96 + \varepsilon)^{0.12}(MPa)$ *Work – Hardened*
		Modulus of Elasticity	E=68.9 GPa
		Poisson's Ratio	0.33

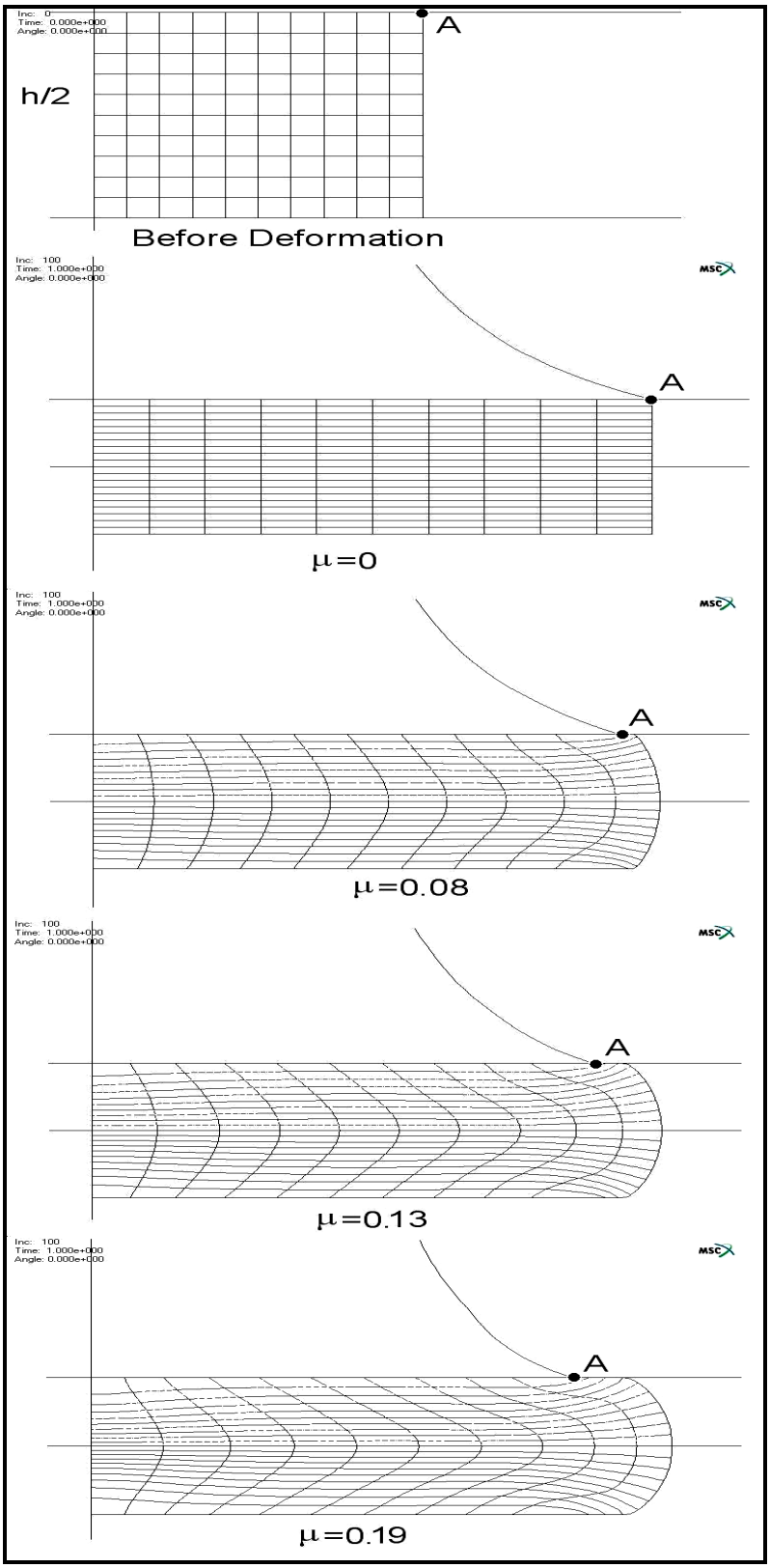

Figure 4.4 Material flowlines and tracked particle positions with different Coulomb coefficients of friction in cylinder upsetting.

The two friction models (Bay's General friction model, Levanov's friction model) which are not available in FEA package was applied with the utility of user subroutine UFRIC in MSC SuperForm. UFRIC is given in Appendix A.

4.1.3: Case Study with Annealed AA-6082

In this section the friction area ratios obtained from FEA will be compared by the experimental data given by Tan [3]. The experimentally determined friction area ratios using cylindrical specimen made of annealed AA-6082 are shown in Figure 4.5 for four different lubricants. While the specimen is upset the reduction in height and R_{10} values were recorded. Tan carried out a numerical experimentation for different coefficient of friction or friction factors. In this case study, FEA results of friction models will be compared with the Tan's experimental and FEA results.

Material model given for annealed AA-6082 is $\sigma = 220 \cdot \varepsilon^{0.19}$ (MPa) and Figure 4.6 shows its flow stress curve. The yield strength for annealed material was taken as 80 MPa. Some mechanical properties of AA-6082 is given in Table 4.2

Table 4.2 Mechanical properties for AA-6082 [37]

Al-Si 1 Mg Mn (AA-6082)		
Yield Stress (MPa)	Tensile Strength (MPa)	Hardness (Vickers)
80 (max)	150 (max)	30-40

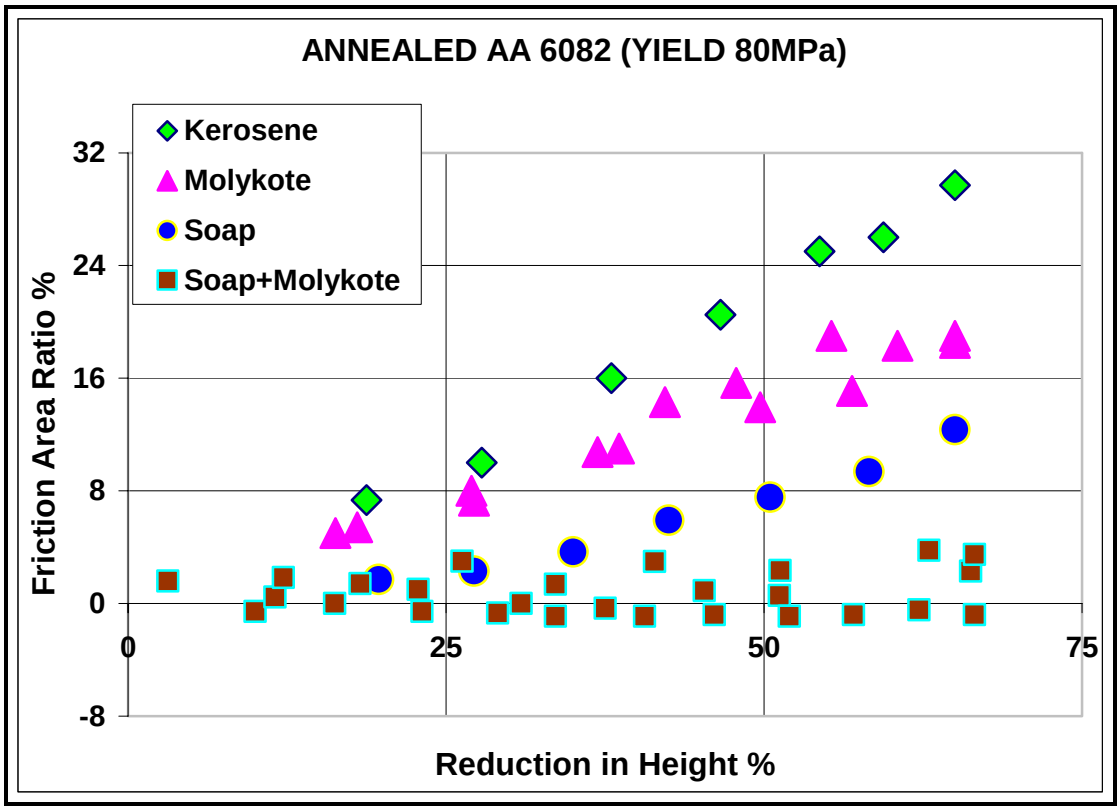

Figure 4.5 Experimentally determined friction area ratios for annealed AA-6082 [3]

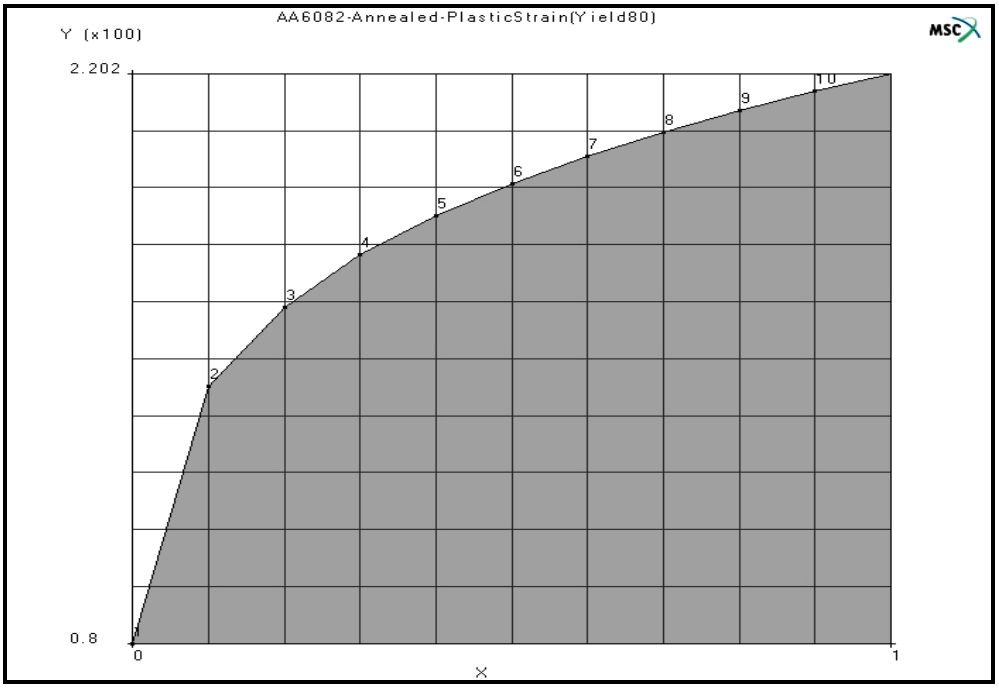

Figure 4.6: True plastic strain - plastic stress curve for annealed AA-6082

The friction area ratios using Coulomb Friction Model is given in Figure 4.7. The values given in parenthesis denote the coefficient of friction used by Tan in numerical experimentation while the others are the values for the best fit curves obtained from the current study for the experimental results. As shown in Figure 4.7, the experimental points obtained using kerosene were fitted to μ=0.165 in Tan's study while in the current study it is achieved with μ=0.19. Similar differences were also observed for the other lubricants.

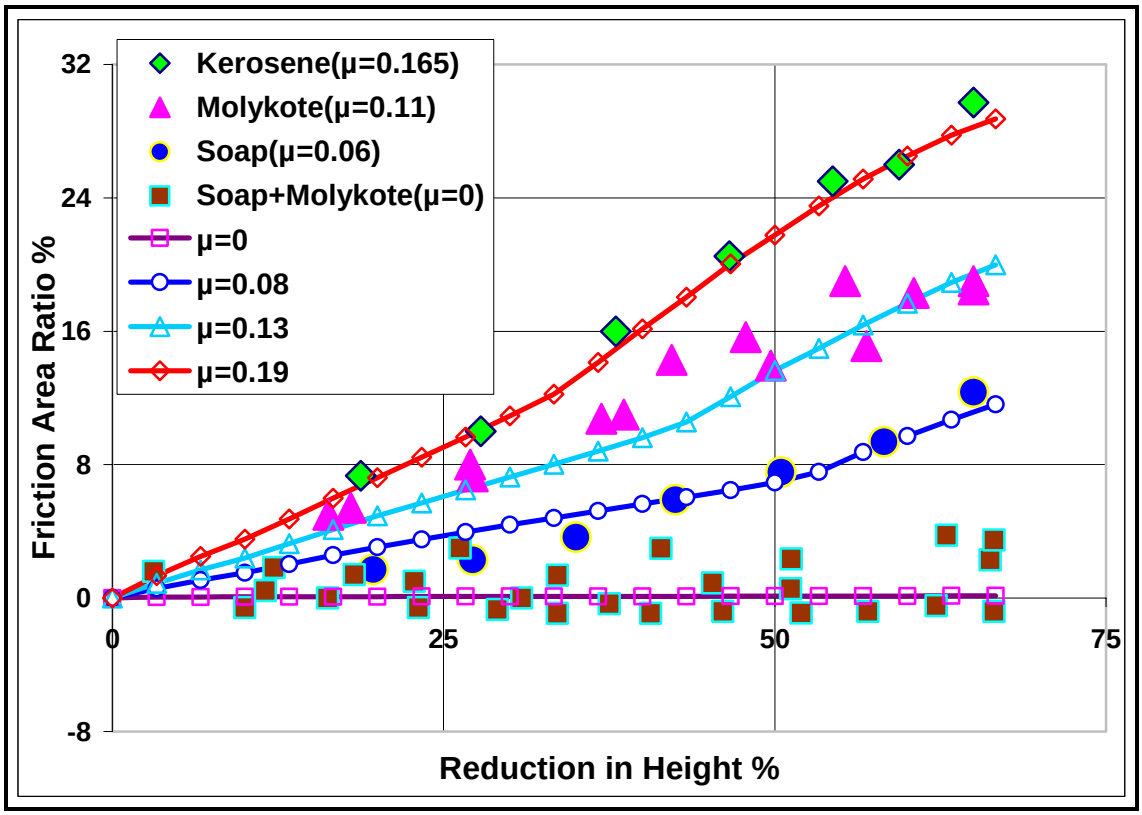

Figure 4.7 Friction area ratios for annealed AA-6082 using Coulomb friction model

Figure 4.8 shows the friction area ratios using Shear friction model in which friction factor is used instead of coefficient of friction. Figure 4.9 shows the friction area ratios using General friction model. Although the Levanov's friction model was not covered in Tan's study, it is included here due to its similarity to the general friction model. Figure 4.10 shows the friction area ratios using Levanov's models.

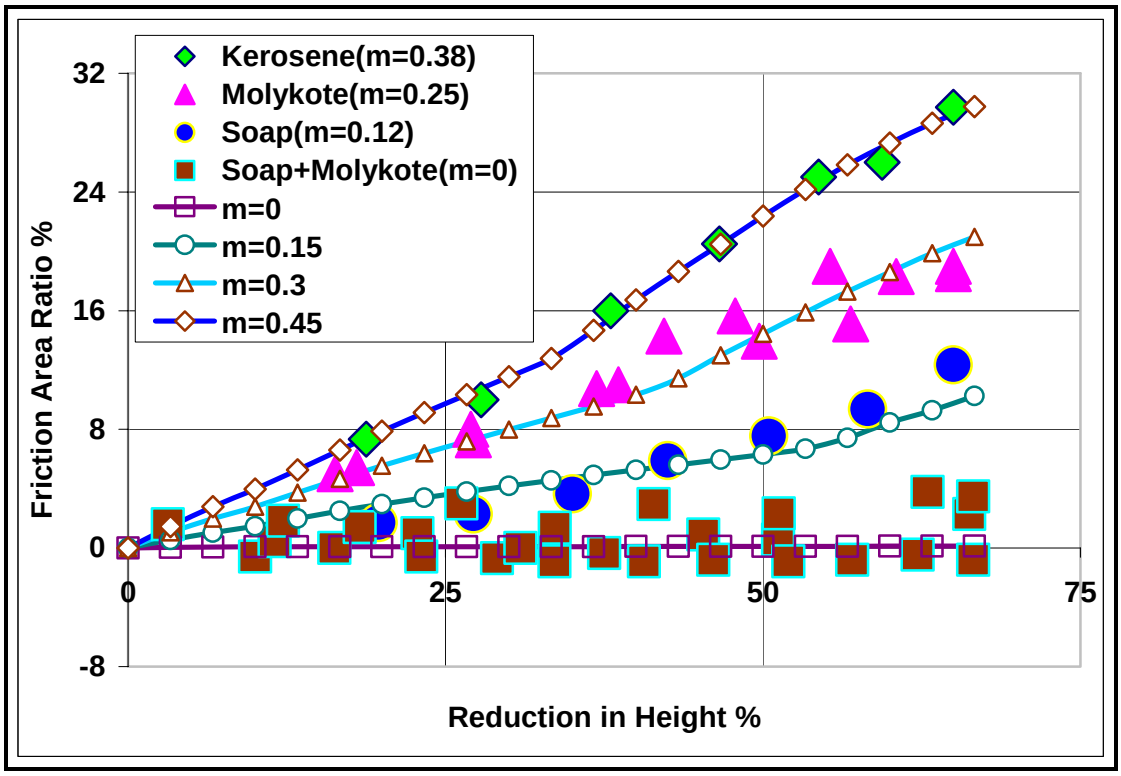

Figure 4.8 Friction area ratios for annealed AA-6082 using Shear (Constant) friction model

There are some differences in Tan's study between the current one. As given in Figure 4.9, the experimental points obtained with soap were curve fit in Tan's study with the friction factor f = 0.3 while the cited points are curve fit with f = 0.7 in current study. Using both Bay's and Levanov's models even with the highest friction factor value (f = 1) in FEA, the experimental points obtained by kerosene couldn't be reached.

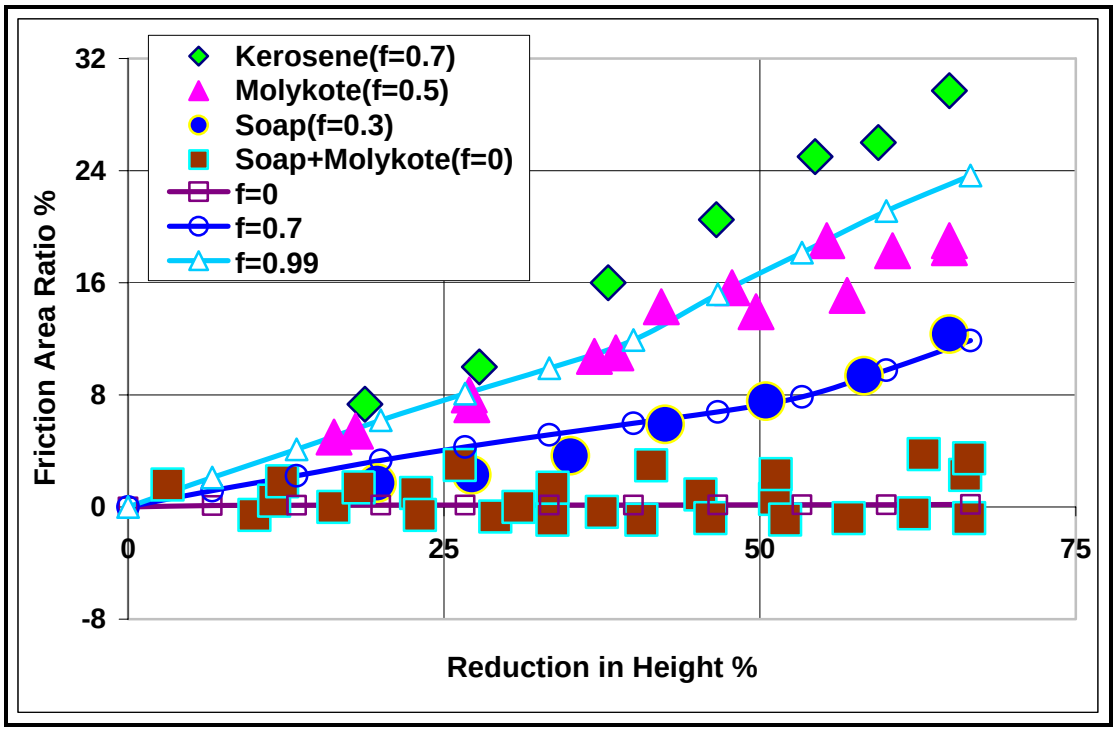

Figure 4.9 Friction area ratios for annealed AA-6082 using General friction model

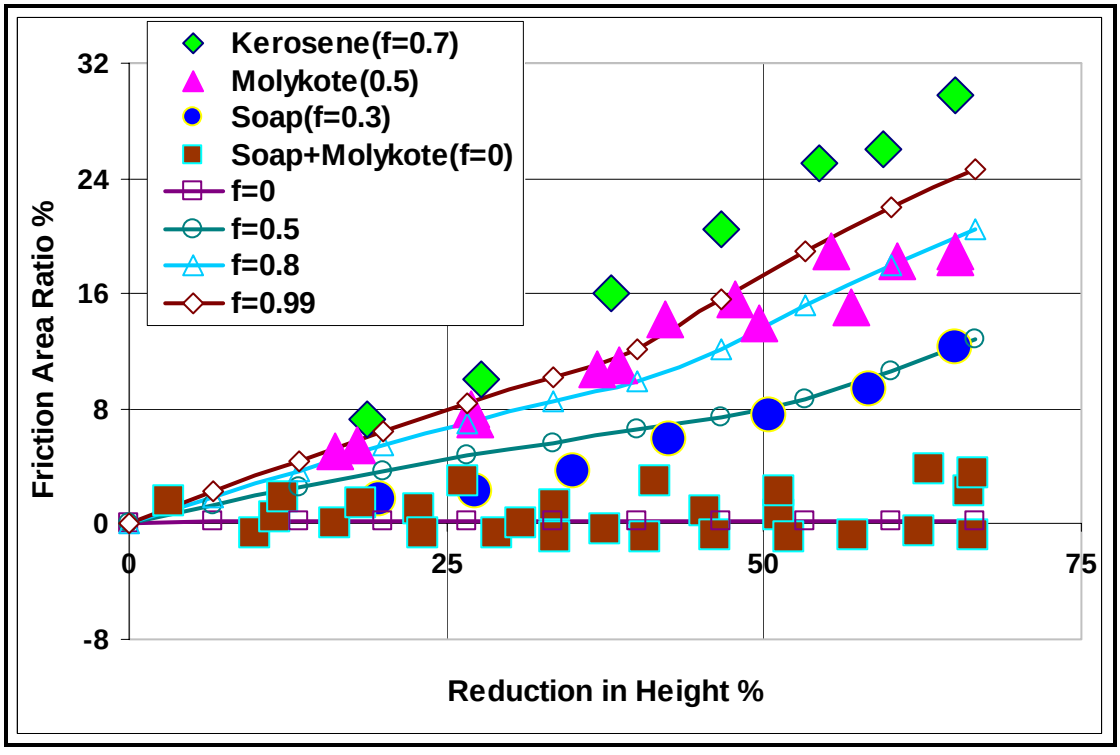

Figure 4.10 Friction area ratios for annealed AA-6082 using Levanov's friction model

4.1.4 Case Study with Work-Hardened AA-6082

Figure 4.11 shows the experiment results obtained by the work-hardened AA-6082. The material model for work-hardened AA-6082 is given as $\sigma = 220(0.96 + \varepsilon)^{0.12}$ MPa . The stress-strain relationship is shown in Figure 4.12.

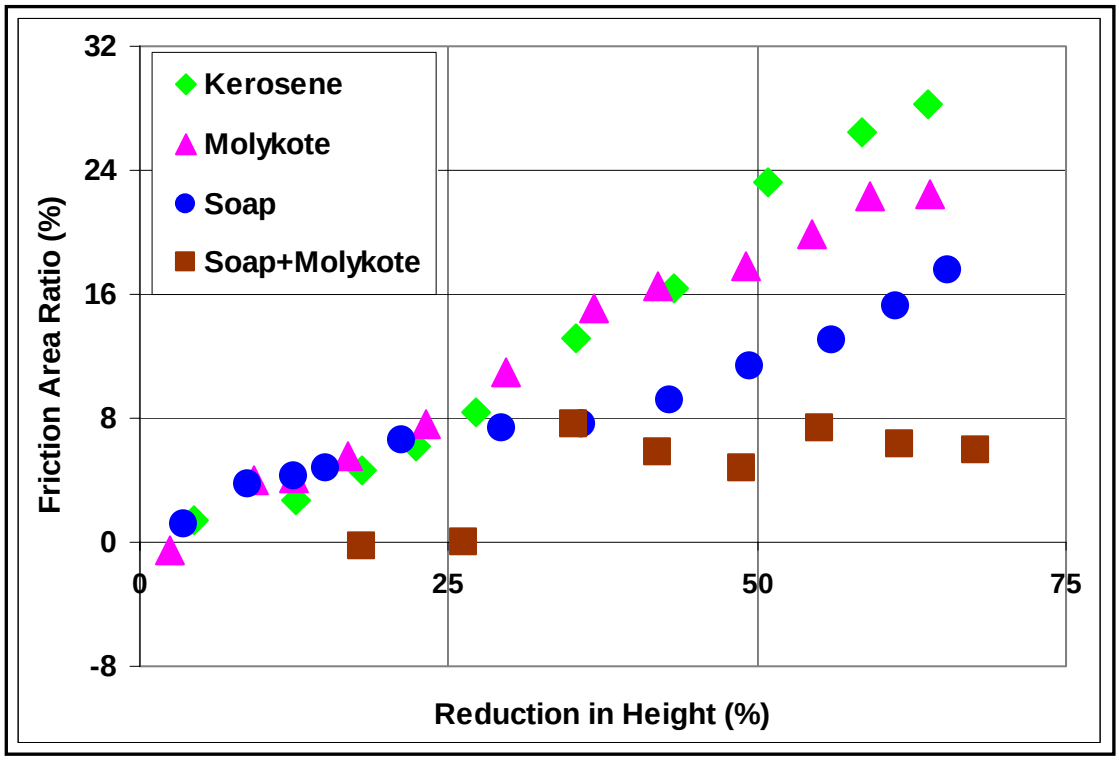

Figure 4.11 Experimentally determined friction area ratios for work-hardened AA-6082 [3]

Friction area ratios for work-hardened AA-6082 using Coulomb, Shear (constant), General (Bay's), Levanov's friction Models are shown in Figure 4.13, 4.14, 4.15, 4.16 respectively.

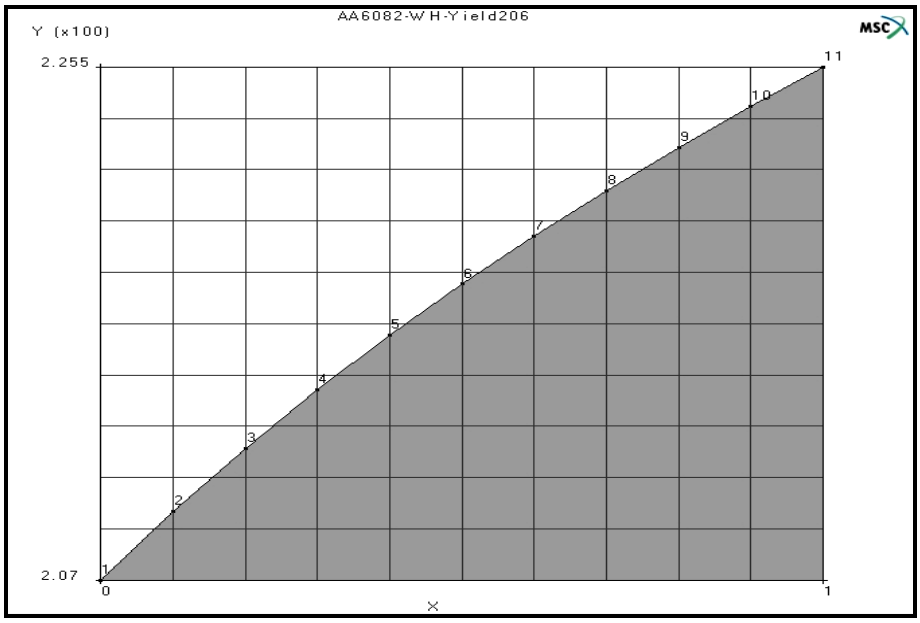

Figure 4.12 Flow stress curve for work-hardened AA-6082

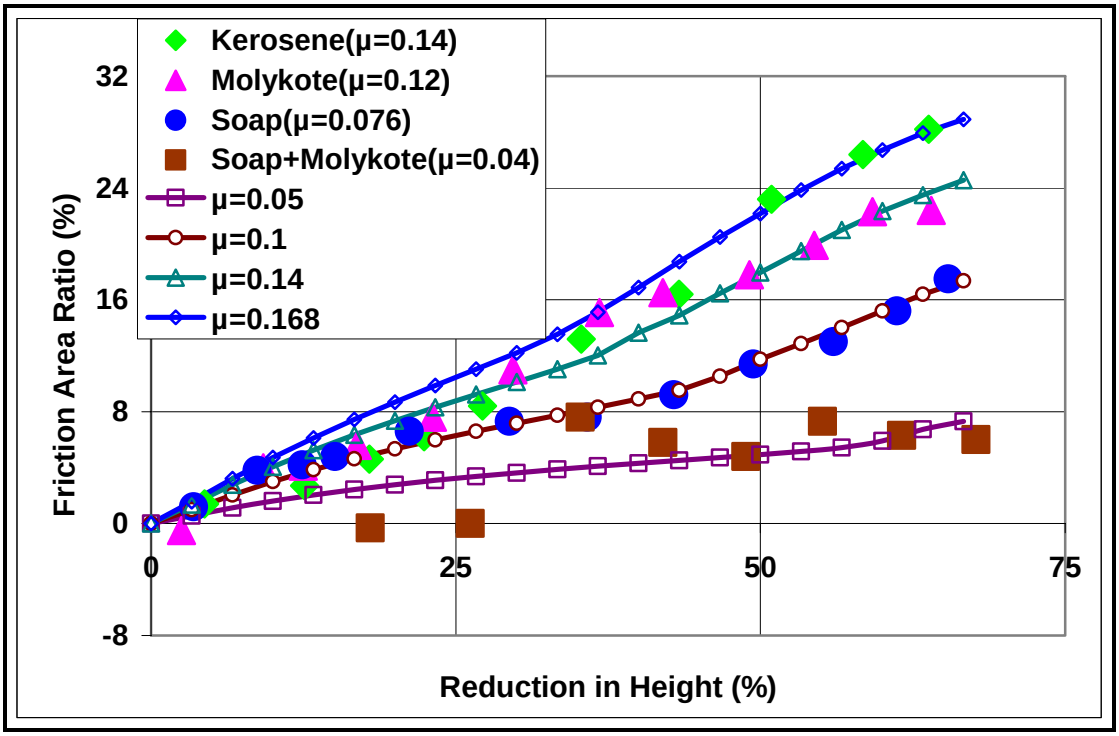

Figure 4.13 Friction area ratios for Work-Hardened AA-6082 using Coulomb friction model

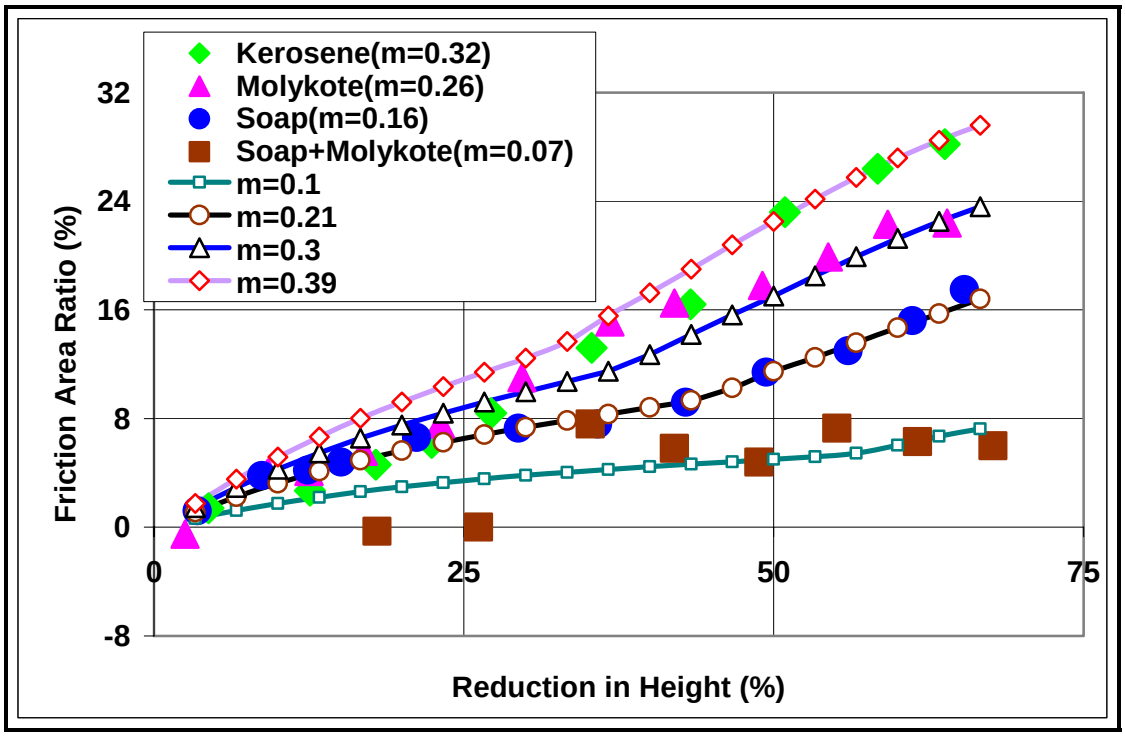

Figure 4.14 Friction area ratios for work-hardened AA-6082 using Shear (constant) friction model

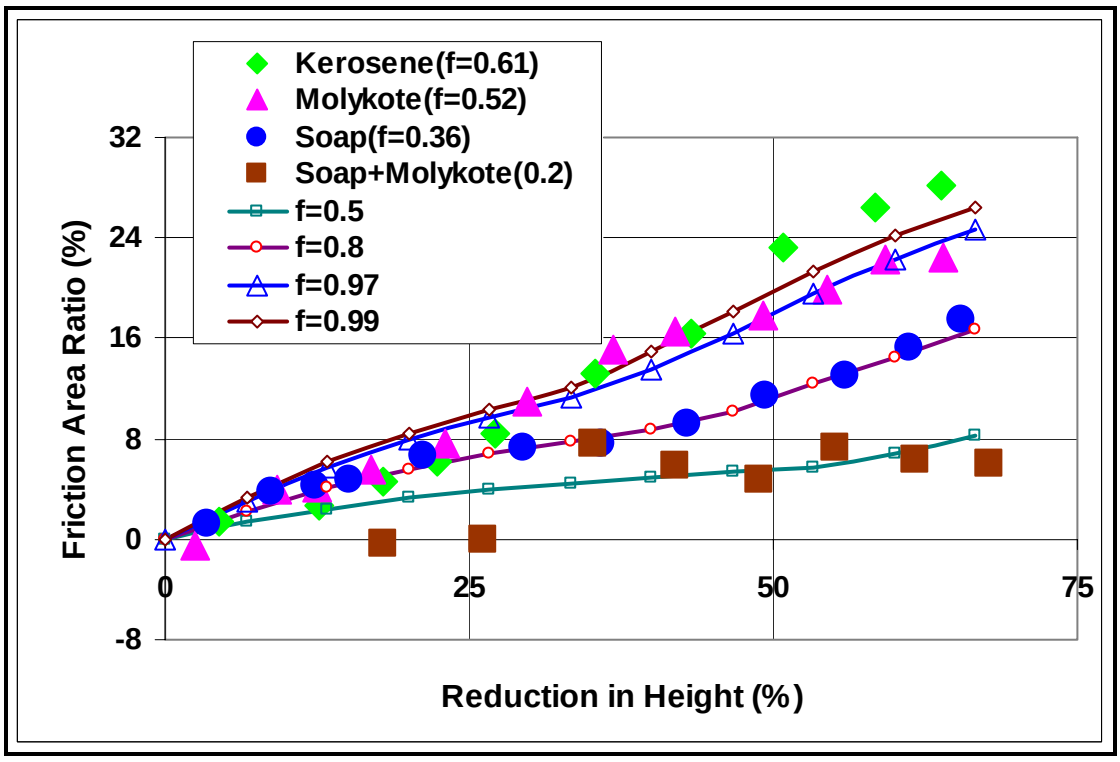

Figure 4.15 Friction area ratios for work-hardened AA-6082 using General friction model

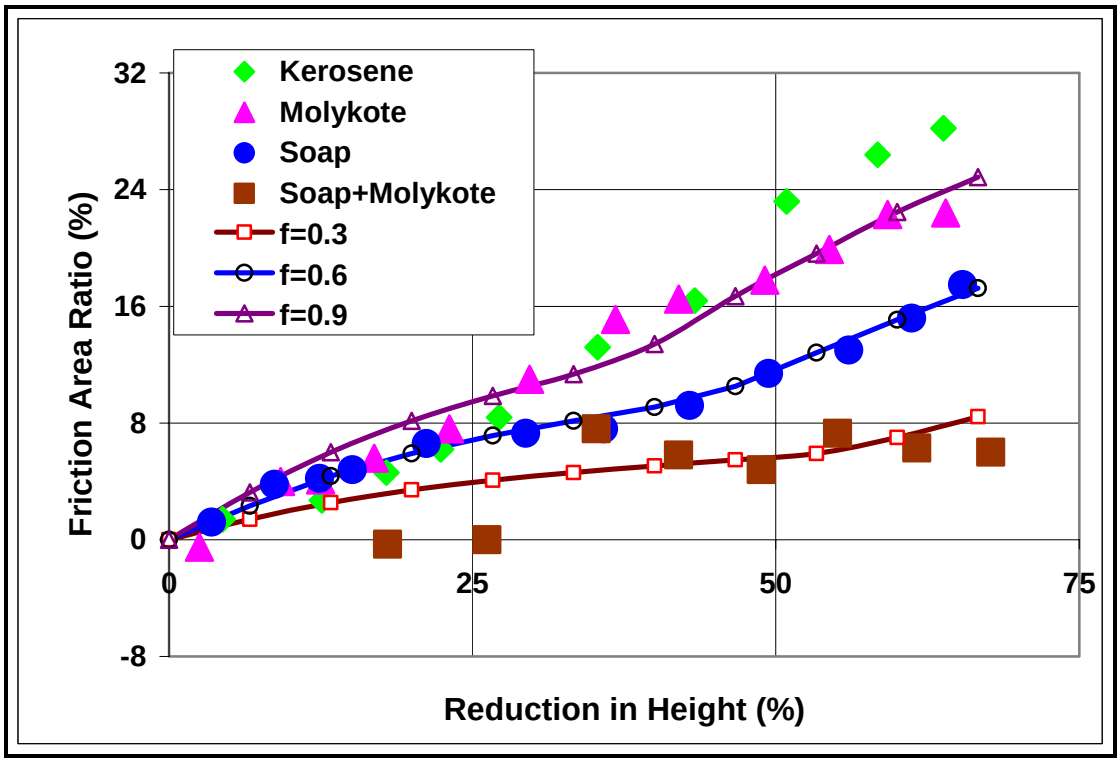

Figure 4.16 Friction area ratios for work-hardened AA-6082 using Levanov's friction model

Similar to annealed material results, in Coulomb and Constant friction models relatively better agreement have been obtained with respect to the results of other friction models. As given in Figure 4.14, the experimental points obtained with molykote were curve fit in Tan's study with the friction factor m = 0.26 while the cited points are curve fit with m= 0.32 in current study. Whereas using both Bay's and Levanov's models, as given in Figure 4.15, Figure 4.16, even with the highest friction factor value (f = 1) in FEA, the experimental points obtained by kerosene couldn't be reached.

4.1.5 Discussion for Case Study I

As expected and recorded in the previous studies, the immigrated contact area and barreling in cylinder upsetting increase with the increasing coefficient of friction or friction factor. It has been also observed that during cylinder upsetting the pressure distribution is almost uniform and is not affected by the friction models applied. Figure 4.17 shows the typical pressure (contact normal stress) distribution on the surface.

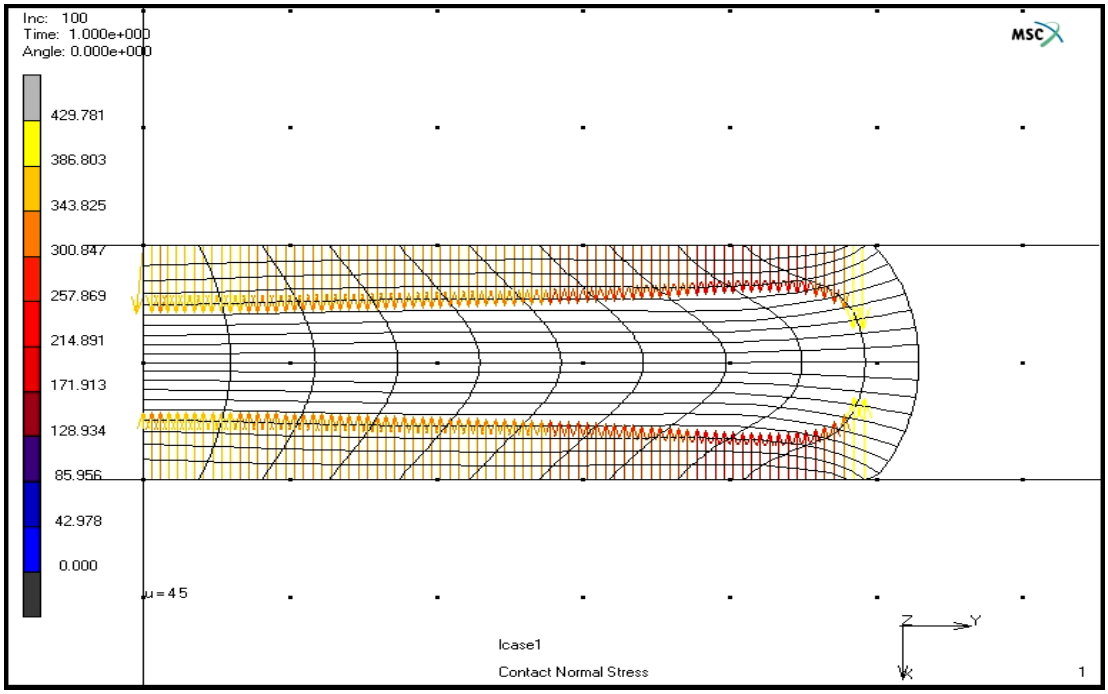

Figure 4.17 Contact pressure distribution of cylinder upsetting using Levanov's friction model (f = 0.7, Height Reduction Ratio: $(h_0 - h_1)/h_0 = 0.67$)

Relatively small differences in FEA analyses have been obtained in Coulomb and Constant friction models compared to other two friction models in both case studies. Tan's FEA were not described in detail and not known. Differences between the results of current and the Tan's study may have been due to the following reasons;

1) In the current study MSC SuperForm version 2004 was used while SORPAS is used in Tan's study. While the SuperForm is specialized in metal forming applications, SORPAS was primarily developed for simulation of resistance welding.

2) Remeshing is important in large strain problems like forging, remeshing characteristics may have contributed to the differences.

4.1.6 Variation of Coefficient of Friction in Case Study I

Figure 4.18 shows the variation of coefficient of friction on the cylindrical billet surface for two different friction models applied on the last step of forming. As can be seen easily there is not any change in friction coefficient with the General friction model. However in Levanov's friction model coefficient of friction is tending to increase from the center to the periphery except the values at periphery.

General friction model gives a constant coefficient of friction on the surface of billet which is due to almost constant contact normal stress to the equivalent yield stress ratio. In Levanov's model coefficient of friction value doesn't take a constant value for specific range of cited ratio. Variation of coefficient of friction in both models and their comparison will be examined in the last headline of this chapter.

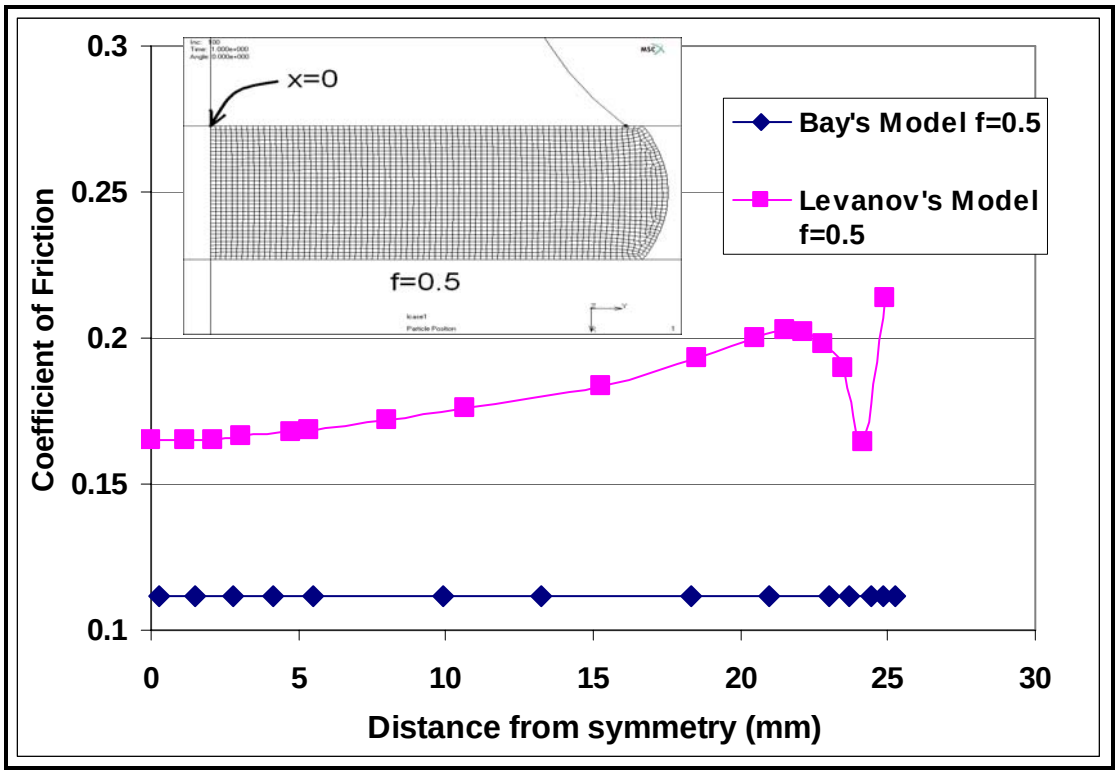

Figure 4.18 Variation of coefficient of friction for two different friction model (f = 0.3, Height Reduction Ratio: $(h_0 - h_1)/h_0 = 0.67$, Work-hardened AA-6082)

4.2 Case Study II

This case study investigates the coefficient of friction and the parameters effecting friction on round bolt head manufacturing. Dimensions for both workpiece and dies are shown in Figure 4.19. Normalized C15 was chosen as the bolt material and its flow stress curve is given in Figure 4.20. In this case study, General friction model and Levanov's friction model will be applied as a friction model. In both General friction and Levanov's models friction factor value f was taken as 0.3. The reasons of this choice will be explained in a detail in discussion part. The reasons of this choice will be explained in detail in discussion part. The FEA results will be given separately for each model.

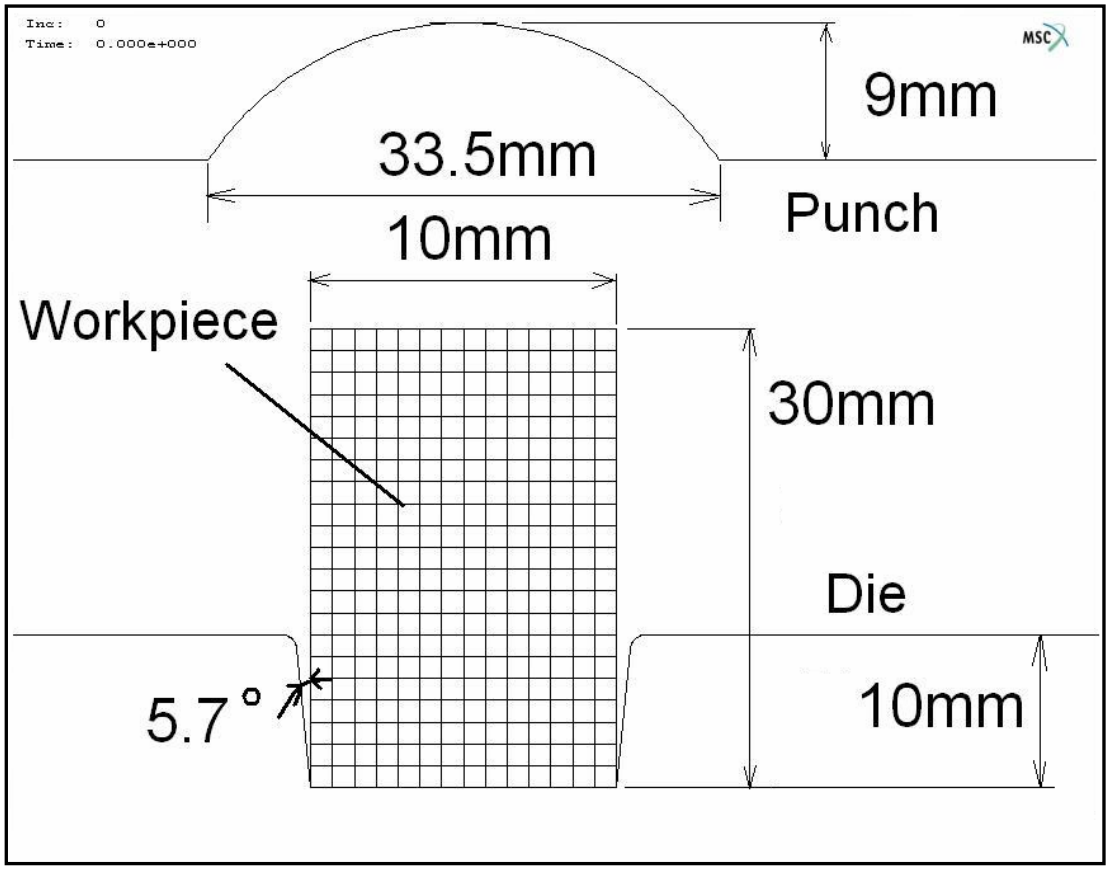

Figure 4.19 Die and workpiece dimensions for case study II

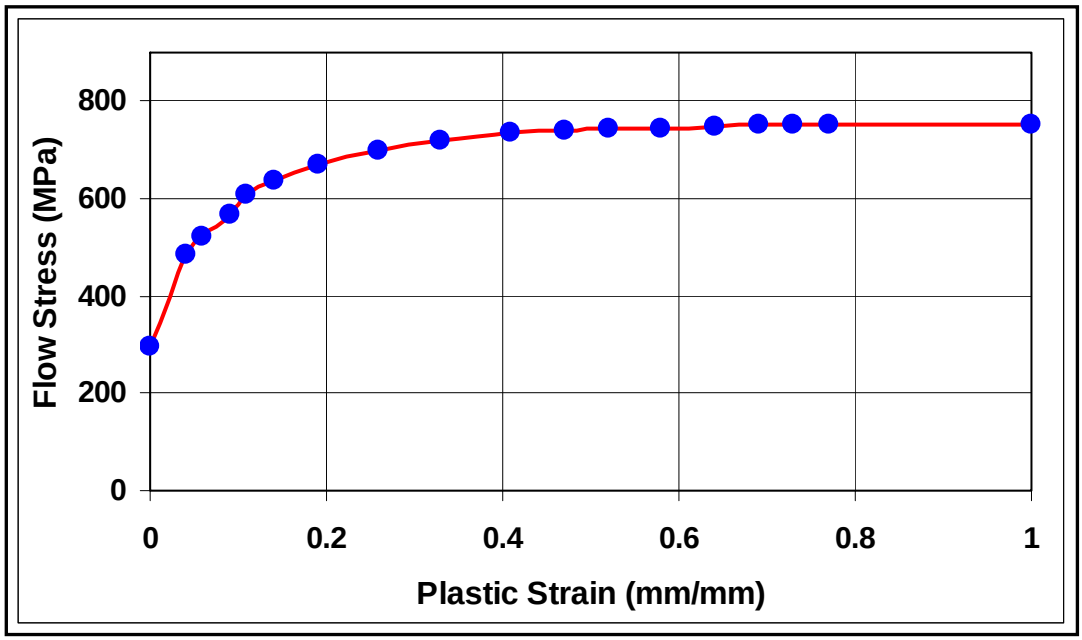

Figure 4.20: Flow stress curve for C15 [38]

Table 4.3 describes options for the FEA. The analysis of 12-mm of punch displacement in forging operation was completed in 120 steps. Advancing front quad type global remeshing was applied. The maximum element edge length after remeshing and the friction factor value chosen significantly affect the solution. For large element edge lengths, to reach a complete solution was not possible.

Figure 4.21 shows the material flowlines and the deformed shape for various steps. The data were collected for these steps given in this figure. As one can see there is less number of nodes in contact with the punch at 30^{th} step. Even in 60^{th} step, the entire upper surface is not in contact with the punch.

Table 4.3 Parameters used in FEA of round bolt head manufacturing

NORMALIZED C 15	ANALYSIS OPTIONS	FEA Program	MSC Marc Mentat Version 2003
		Compiler for User Subroutines	Digital Fortran v.6.6
		Material Plasticity Procedure	Elastic-Plastic
		Die Material Type	Rigid
		Punch Velocity	1 mm/s
		Number of Steps	120
		Time per Step	0.01 s
		Iteration Method	Newton-Raphson
		Remeshing	Global remeshing, advancing front quad type, depends on element distortion, angle deviation: 40˚
		Max. Element Edge Length After Remeshing	0.4 mm
		Number of Elements	Half model: 147(at start) - ~2000(max.)
	CONTACT	Friction Models	Bay's (general), Levanov's models
		Relative Sliding Velocity	Default (=0)
		Coefficient of Friction	variable in Bay's and Levanov's (Friction factor f=0.3)
		User Subroutine	UFRIC
	Material	Modulus of Elasticity	Default values from material library of MSC Marc Mentat
		Poisson's Ratio	

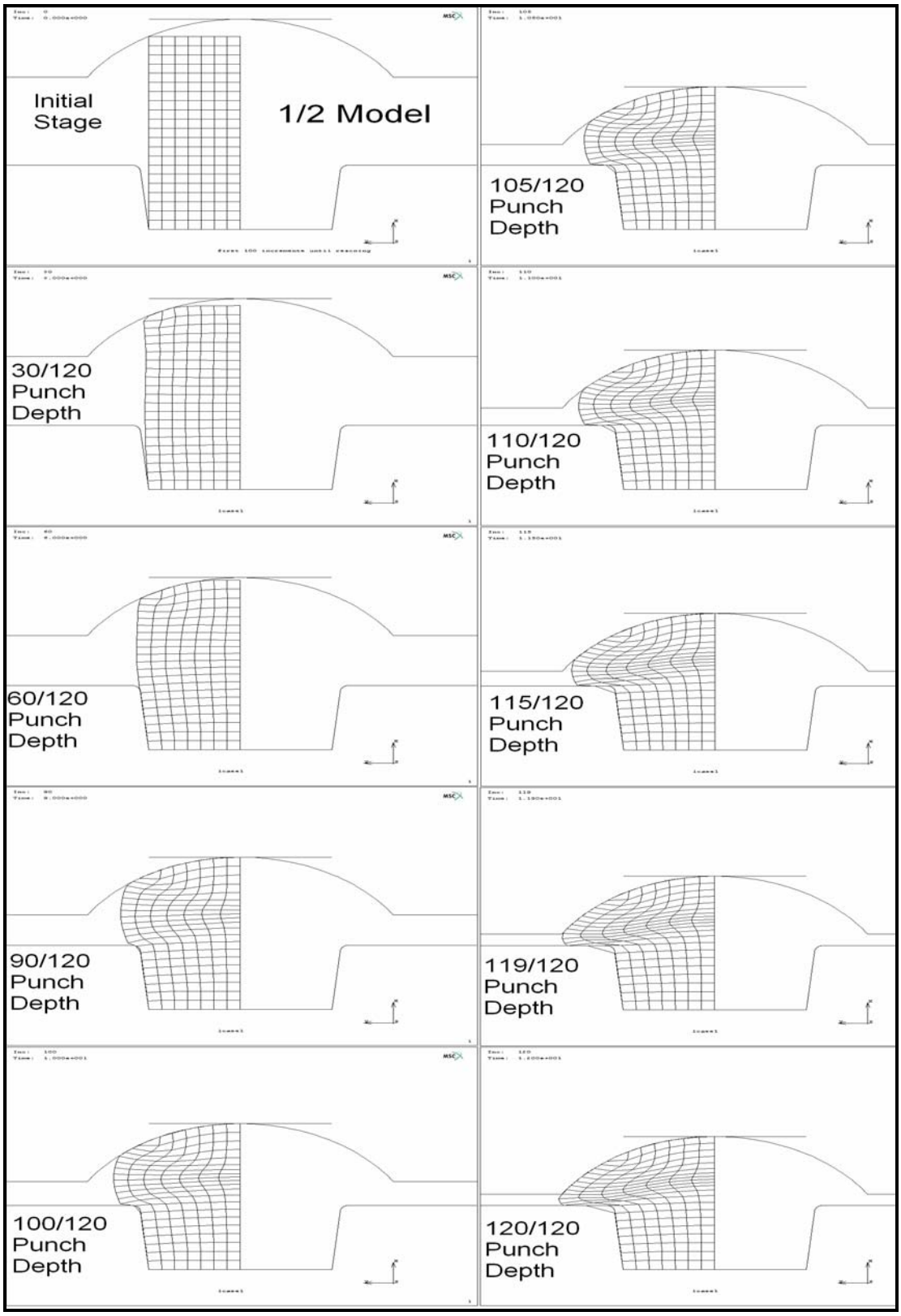

Figure 4.21 Material flowlines and deformed shapes of half model for various steps in case study II

4.2.1 Results with General Friction Model

As specified in Table 4.3 the analysis was completed in 120 steps. To compare the results on the bolt head, the output values were recorded in 9 different steps. Relatively small deformations occurred in the first 60 steps and head shape formation was in early stages and the contact did not reach to the centre. Therefore, less number of nodes was in contact with the punch and the output values were also recorded in 30^{th} and 60^{th} steps. In addition to those initial steps, the output values recorded for 90^{th} step. Towards the last increments the bolt head formation increases. Therefore, the output values at 6 different increments (100,105,110,115,119,120) were recorded.

Figure 4.22 shows variation of the contact normal stress for different steps. In 30^{th} and 60^{th} steps relatively less number of points was in contact with the punch. The values for these two steps show significant deviations. That can be explained by due to the stagnant material during head forming.

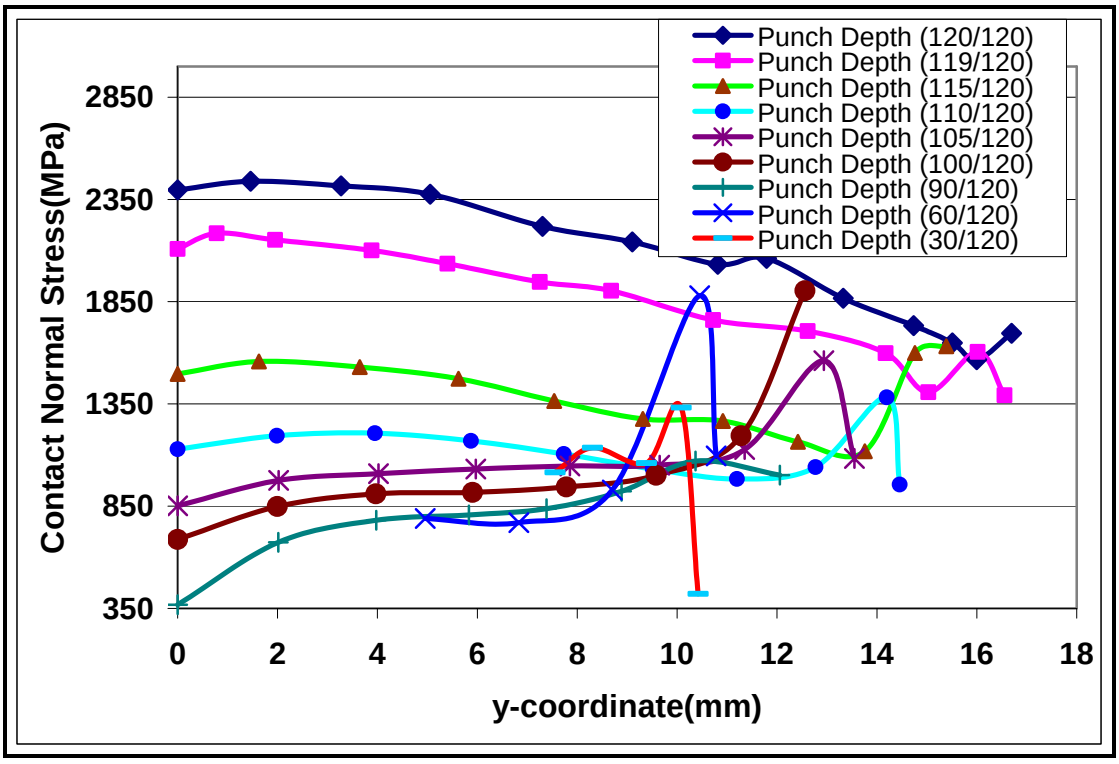

Figure 4.22 Variation of contact normal stress on the head of bolt with General friction model

Figure 4.23 shows the variation of the ratio of contact normal stress to the equivalent yield stress (q/σ_0). On the central part of the head, the ratio is about 1.5 up to 105th step and then increases steadily up to the last step. The coefficient of friction is constant up to a certain ratio of (q/σ_0), as can be seen in Figure 4.24. On the head of the bolt, the central part of the contact surface for 60th step and the entire contact surface for 90th step, the coefficient of friction value is converged to a specific value which is about 0.06. This is the maximum coefficient of friction value for f = 0.3 in General Friction Model. If the Figure 4.23 is reviewed again, one can easily see that the ratio of (q/σ_0) for contact surface is below 1.5 and gives a constant coefficient of friction.

Figure 4.25 shows the variation of relative sliding velocity along the forging process. The most significant characteristic is that it tends to increase towards the periphery of the head.

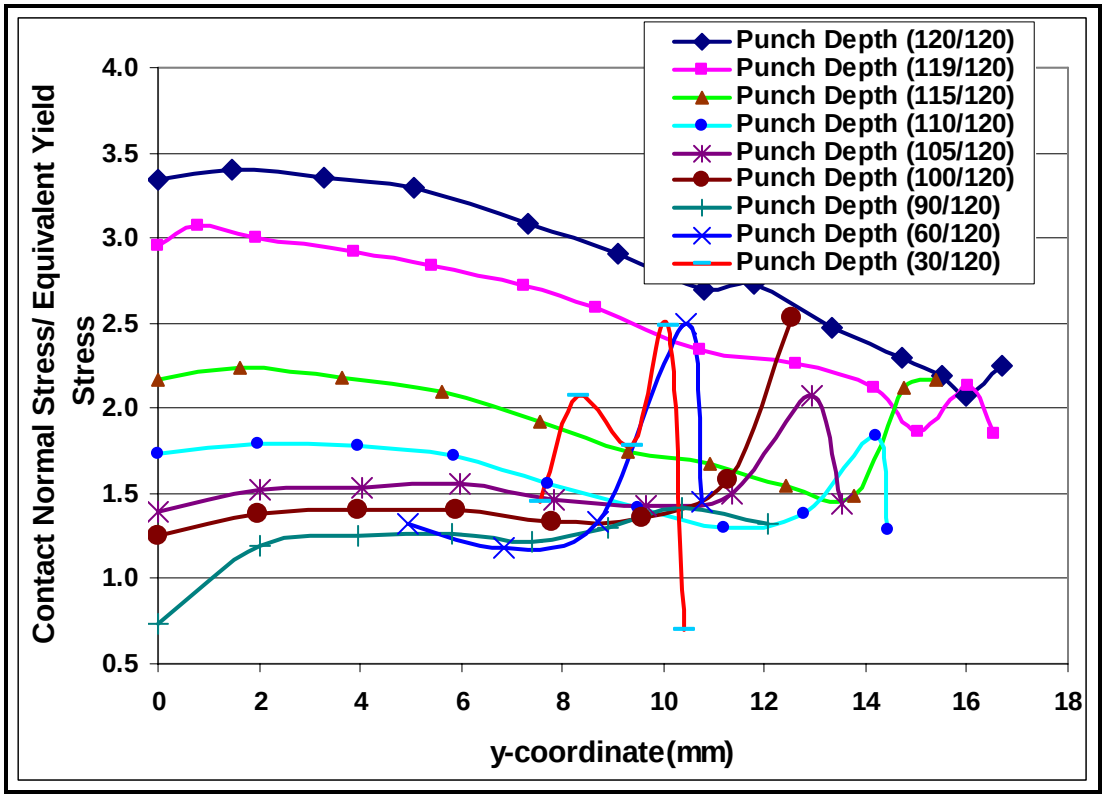

Figure 4.23 Variation of contact normal stress / equivalent yield stress ratio with General friction model

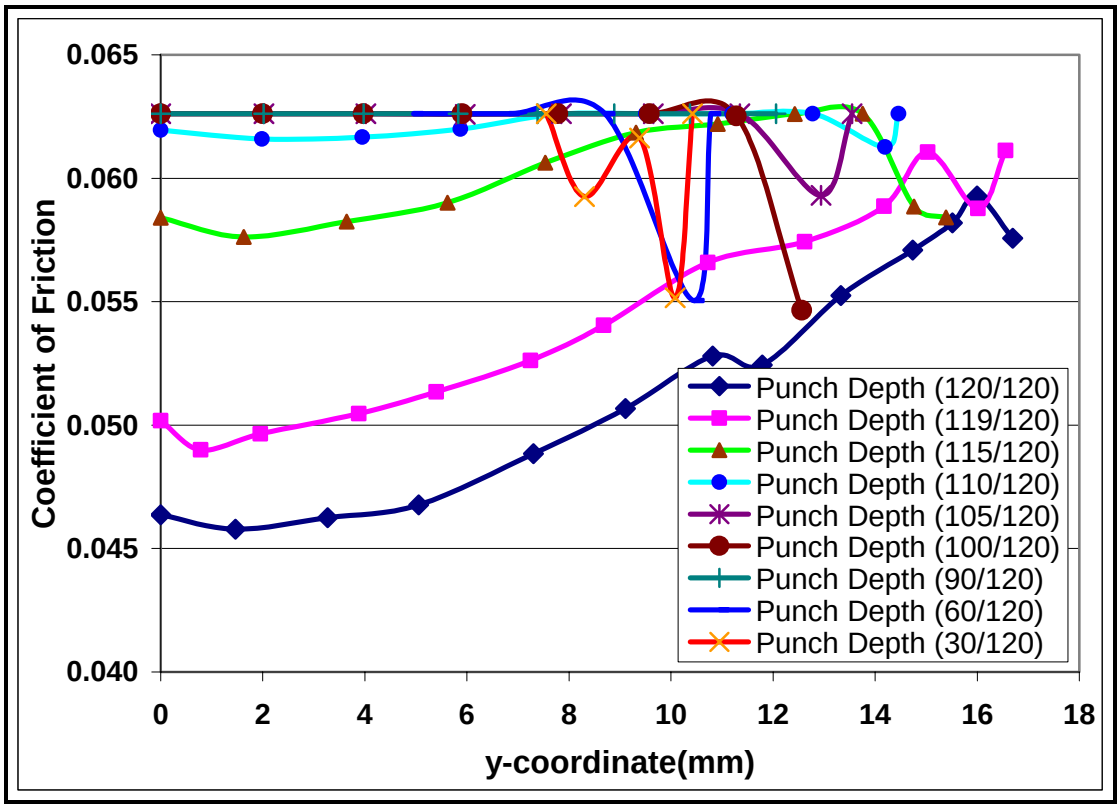

Figure 4.24 Variation of coefficient of friction on the head of bolt with General friction model

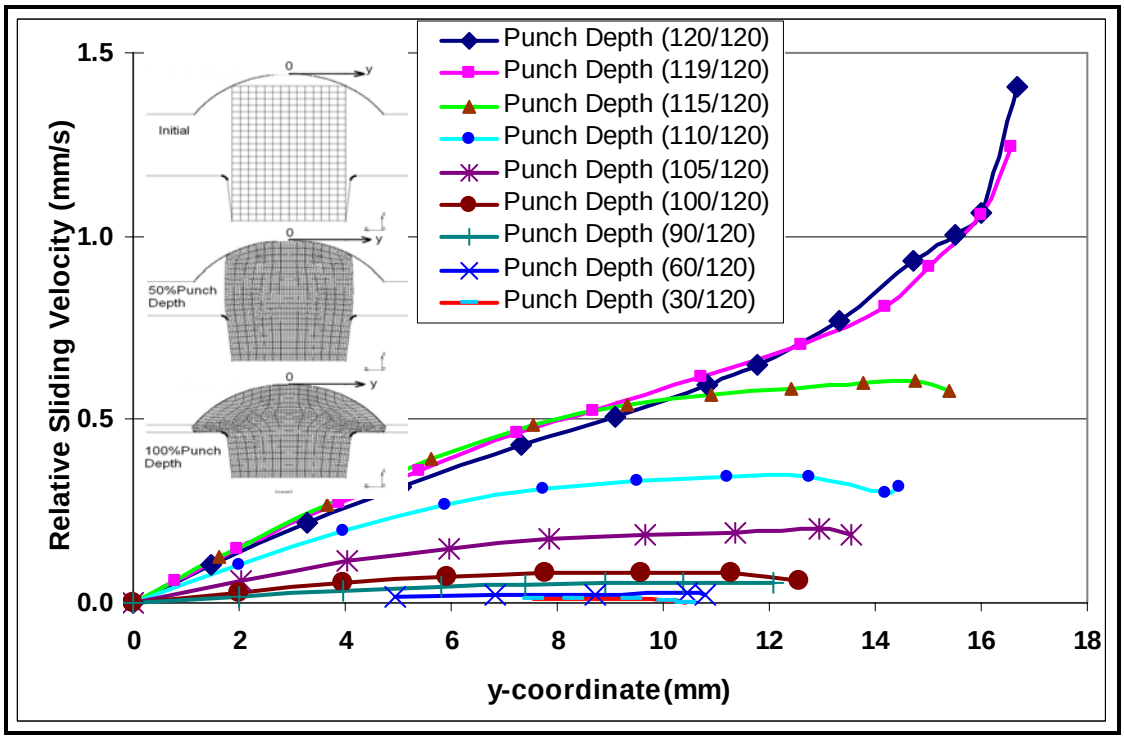

Figure 4.25 Variation of relative sliding velocity on the head of bolt with General friction model

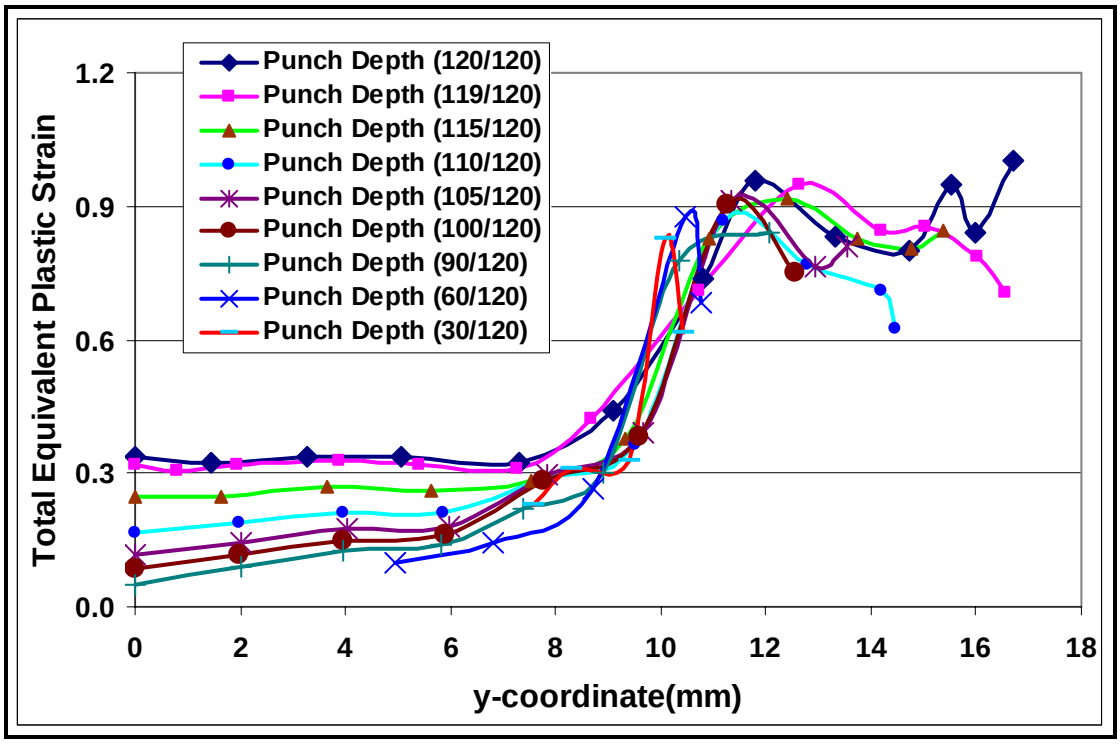

Figure 4.26 Variation of total equivalent plastic strain on the head of bolt with General friction model

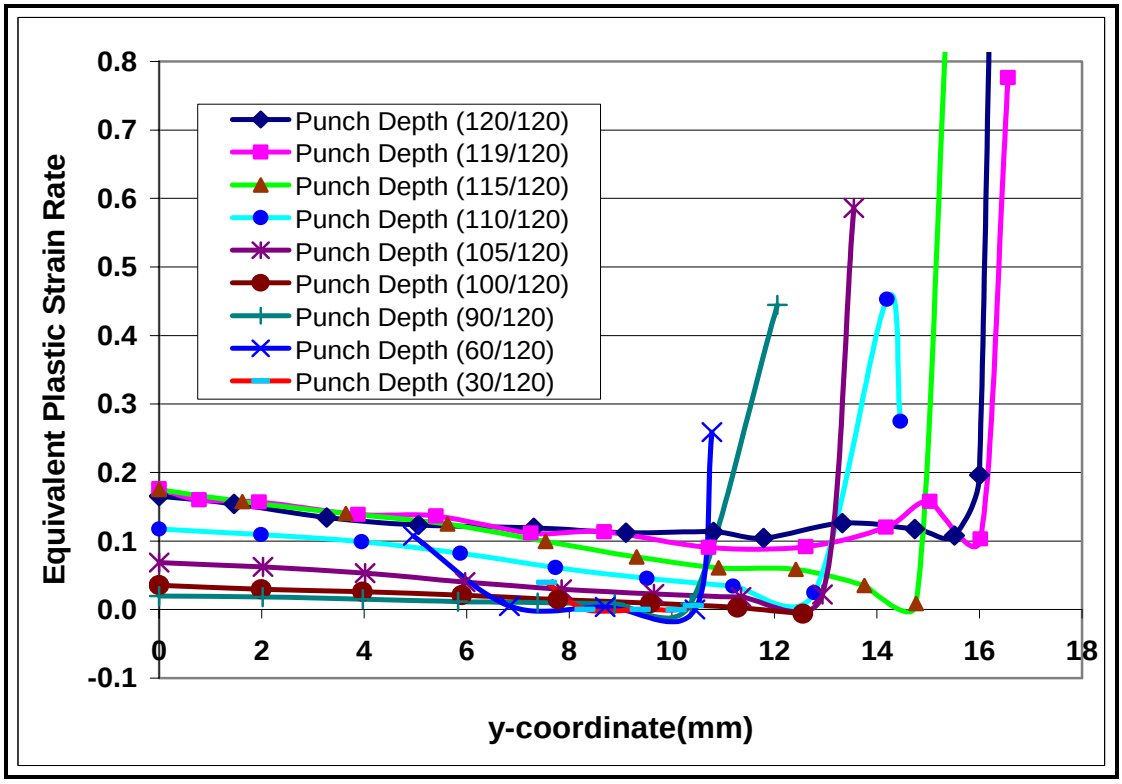

Figure 4.27 Variation of equivalent plastic strain rate on the head of bolt with General friction model

Figure 4.26 shows the variation of total equivalent strain while the Figure 4.27 shows the variation of equivalent plastic strain rate. General characteristics of both curves are similar except that there is a significant increase on the equivalent plastic strain rate curves at the periphery of the head. That could be due to the highest velocity of the nodes at periphery, since there is not any material pile on the front that impedes the advancement of the material flow.

Figure 4.28 denotes the variation of von-Mises equivalent stress which is an important parameter in terms of understanding global stress state of material. Except the values at 30th and 60th steps, on the central part of the head the equivalent von-Mises stress increases steadily and approaches to the stressat the periphery which is about 750 MPa.

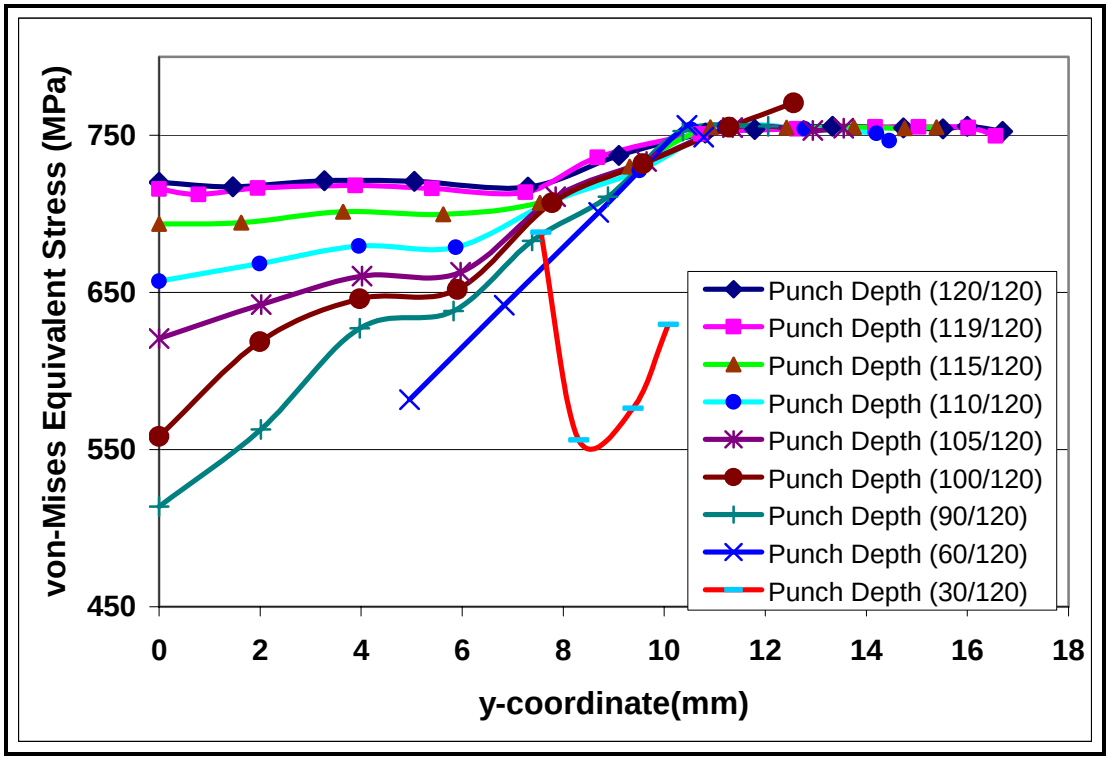

Figure 4.28 Variation of von-Mises equivalent stress with General friction model

Figure 4.29 and Figure 4.30 show the von-Mises equivalent stress on the 30th and 60th steps. On the initial stages of forging, the upper surface of the cylinder is not fully in contact with the punch. Due to high stresses on a small contact region, high contact stress variations are observed.

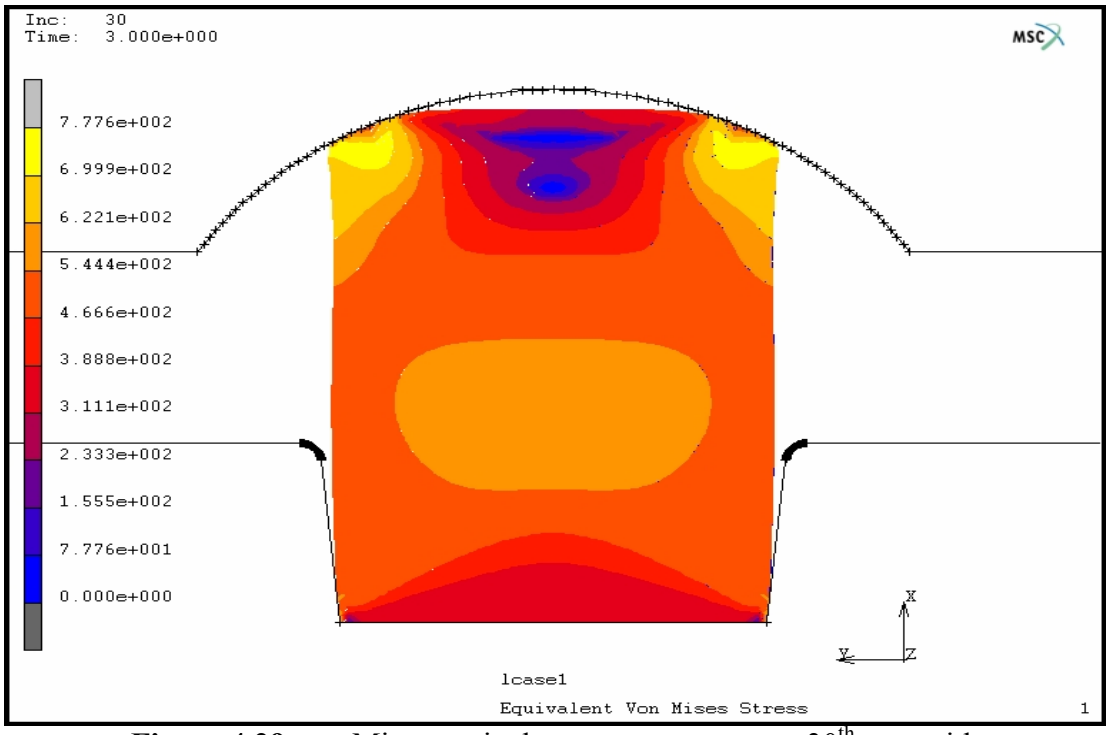

Figure 4.29 von-Mises equivalent stress contours at 30th step with General friction model

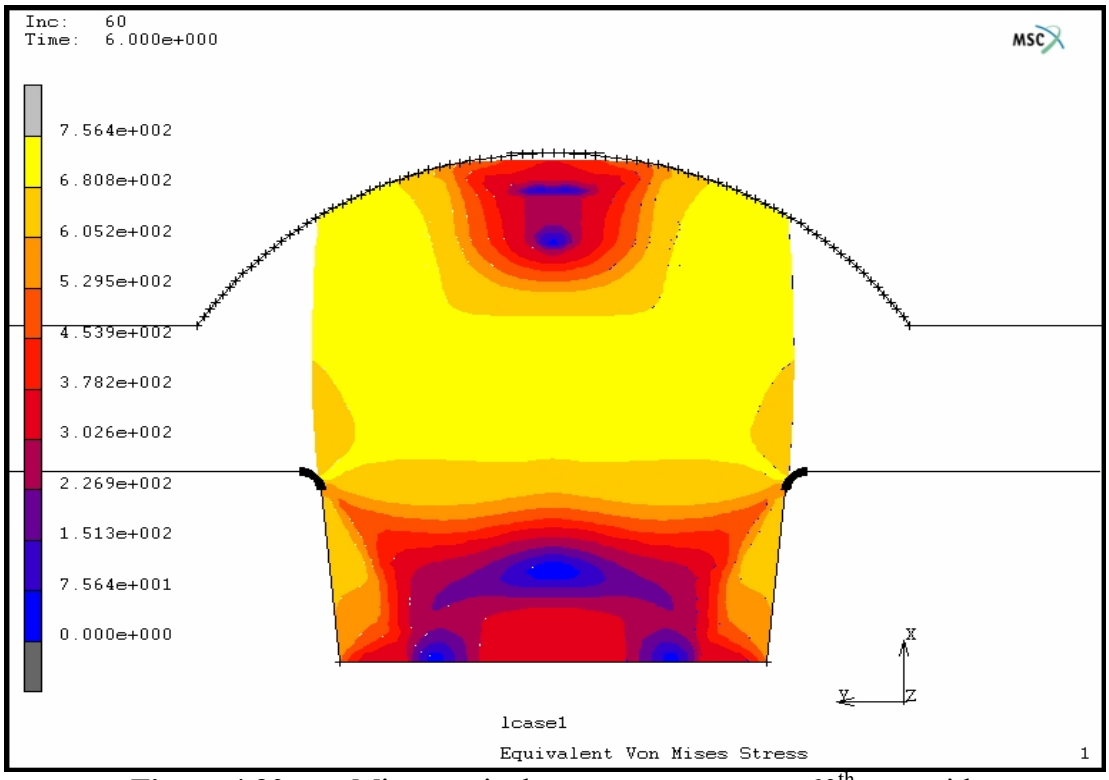

Figure 4.30 von-Mises equivalent stress contours at 60th step with General friction model

4.2.2 Results with Levanov's Friction Model

The FEA results obtained by using Levanov's friction model are shown in Figure 4.31 through Figure 4.38. Figure 4.30 denotes the variation of contact normal stress on the contact surface along the forging process. In general, the contact starts on the periphery of the cylindrical billet and proceeds towards the centre. Initially, the contact pressure on the central part is lover than the periphery, then it starts to increase and finally it becomes higher than the contact pressure on the periphery. In the last two steps shown (119^{th} and 120^{th} steps), the bolt head cavity completely filled and the flash formation is to start at the small gap between the die and punch giving the highest-pressure value on the periphery of the bolt head. The contact normal stress variations are almost the same in both Bay's and Levanov's friction models. Similar to the Bay's results, there is significant variation 30^{th} step. Figure 4.32 shows the vector plot of contact normal stress contours for four different steps.

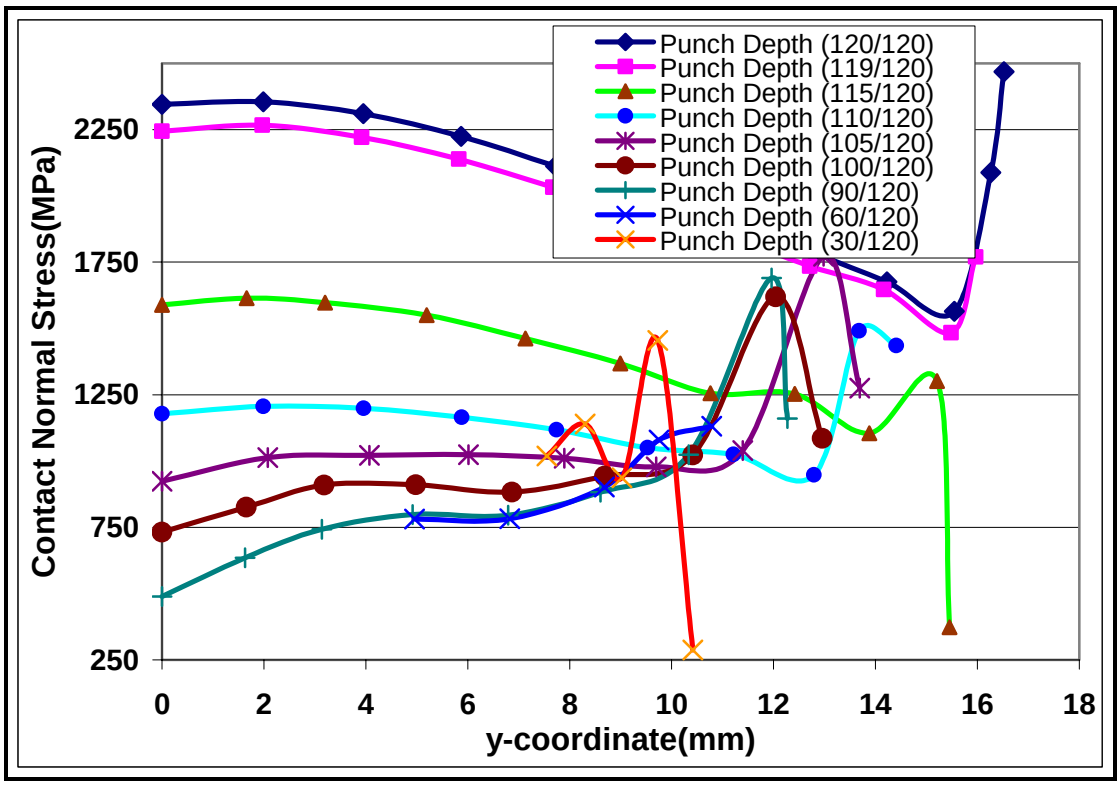

Figure 4.31 Variation of contact normal stress on the head of bolt with Levanov's friction model

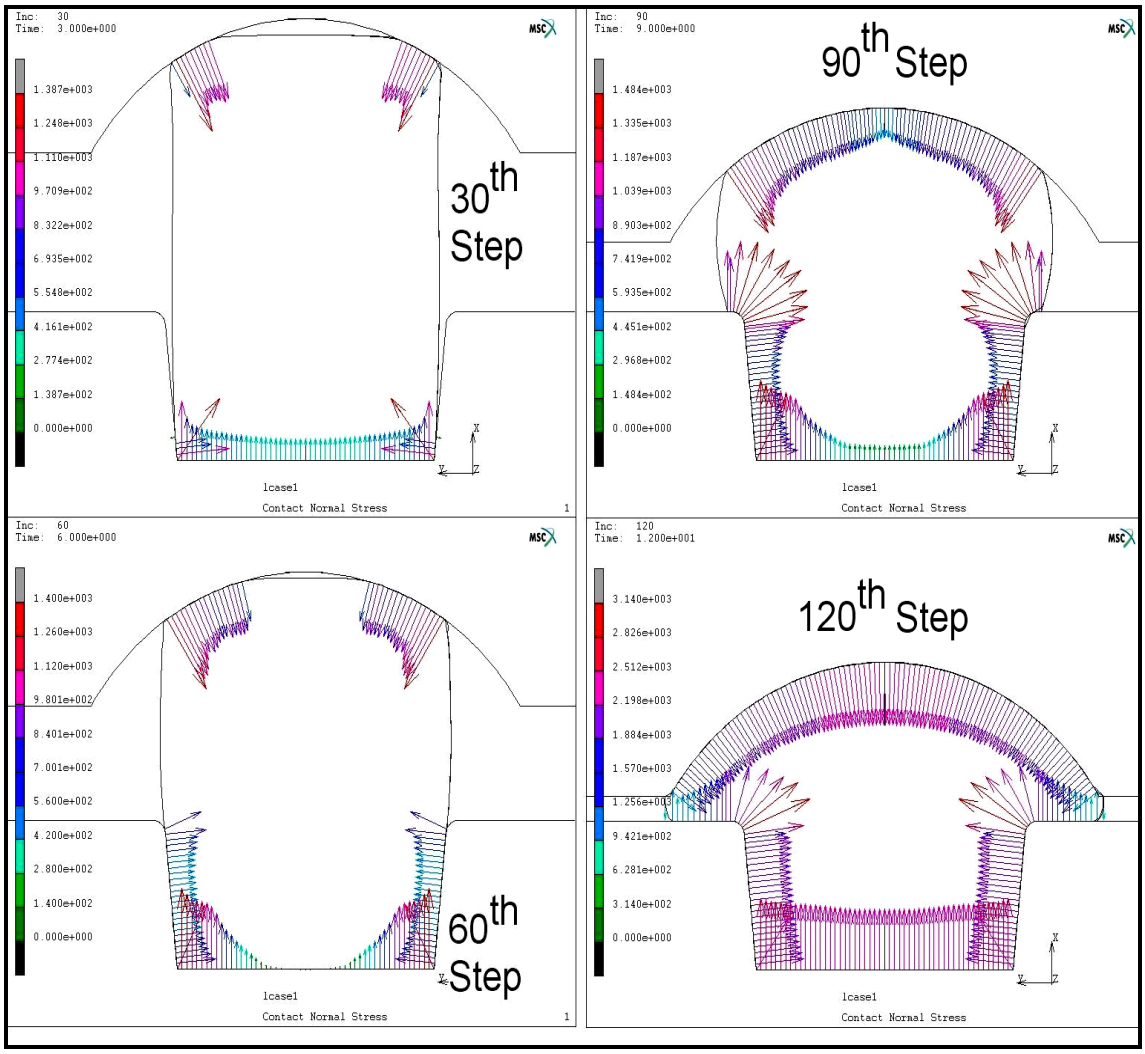

Figure 4.32 Vector plot of contact normal stress for 4 different steps.

Figure 4.33 shows the variation of q/σ_0 while Figure 4.33 shows the variation of coefficient of friction.

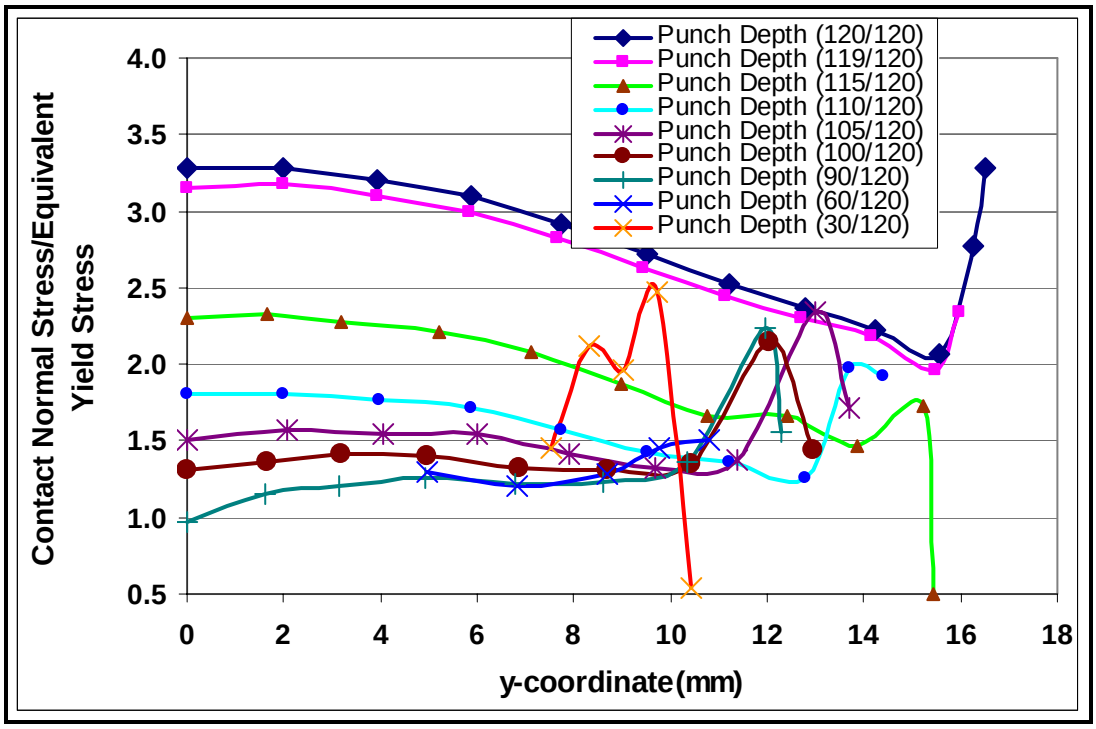

Figure 4.33 Variation of contact normal stress / equivalent yield stress ratio with Levanov's friction model

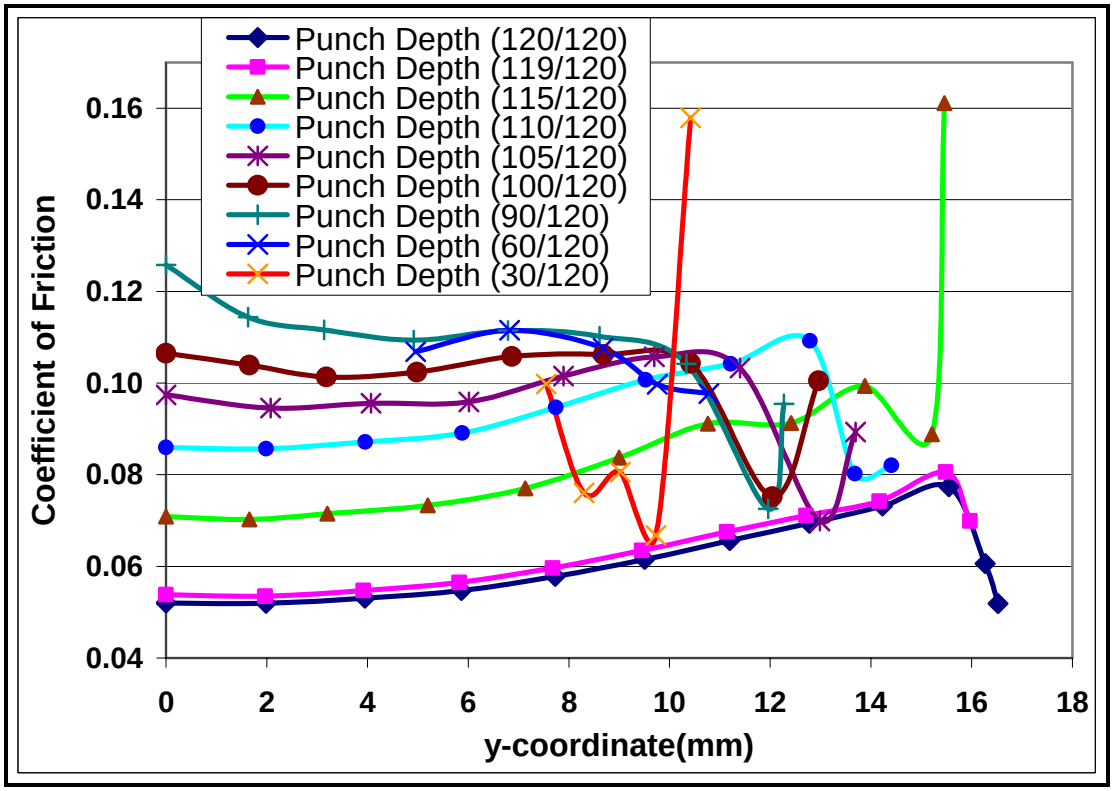

Figure 4.34 Variation of coefficient of friction on the head of bolt with Levanov's friction model

While the maximum coefficient of friction is about 0.06 in Bay's model,, it can reach to about 0.16 as seen in Figure 4.34. Moreover the range of coefficient of friction is larger than the one in Bay's model.

As explained before, the coefficient of friction at the periphery of the head is higher than the central part. Figure 4.35 shows the variation of relative sliding velocity along the forging process. It is similar to results obtained by using Bay's friction model.

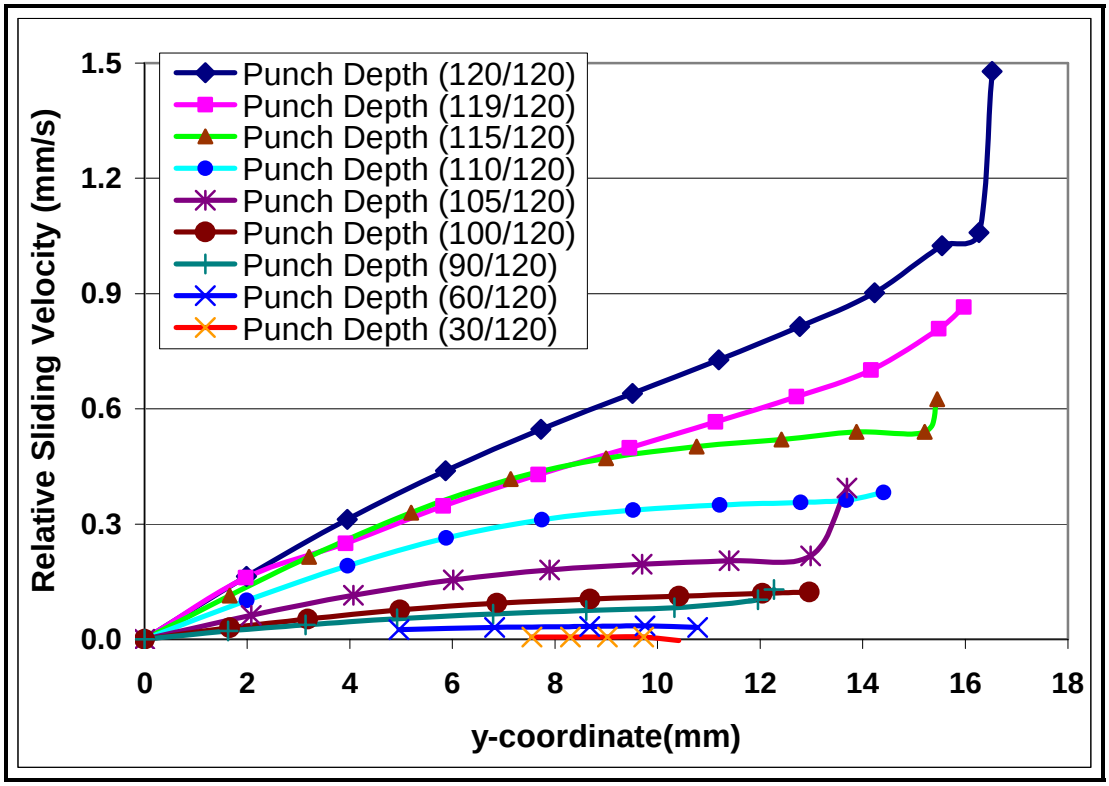

Figure 4.35 Variation of relative sliding velocity on the head of bolt with Levanov's friction model

Figure 4.36 shows the variation of total equivalent plastic strain while the Figure 4.37 shows the variation of equivalent plastic strain rate. Characteristics of these two curves do not differ much from the results obtained by using Bay's friction model.

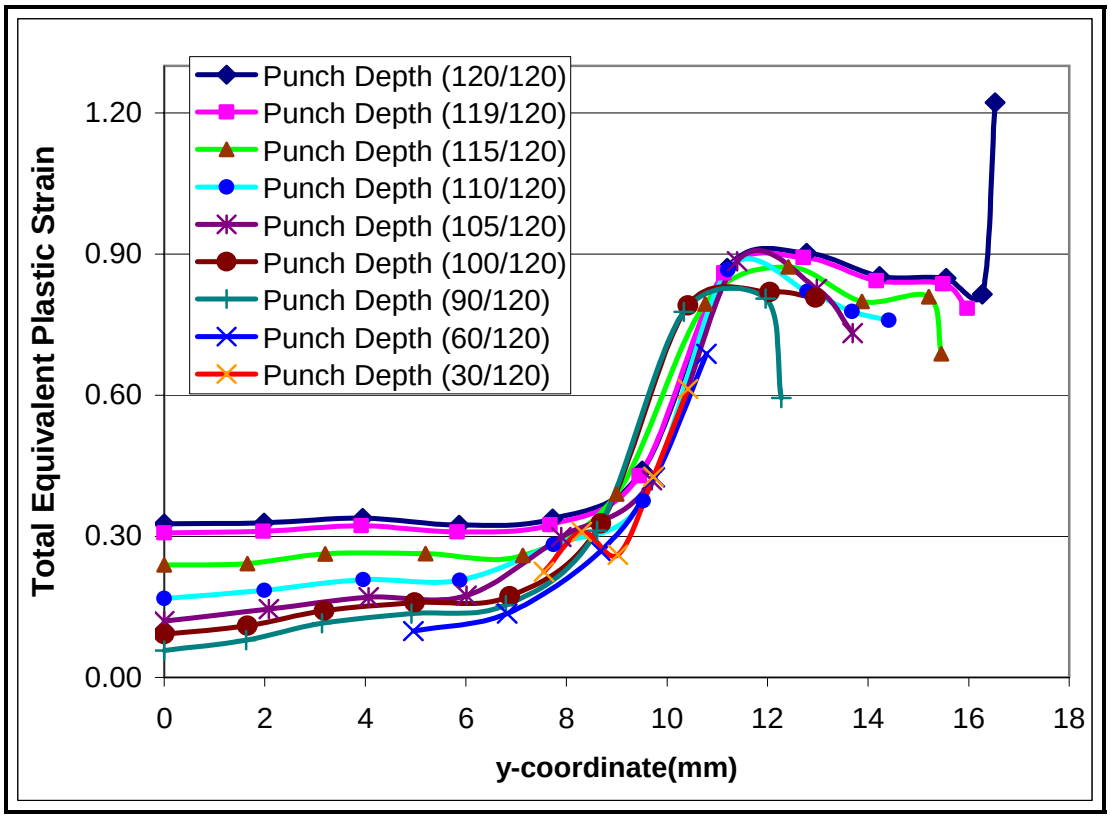

Figure 4.36 Variation of total equivalent plastic strain with Levanov's friction model

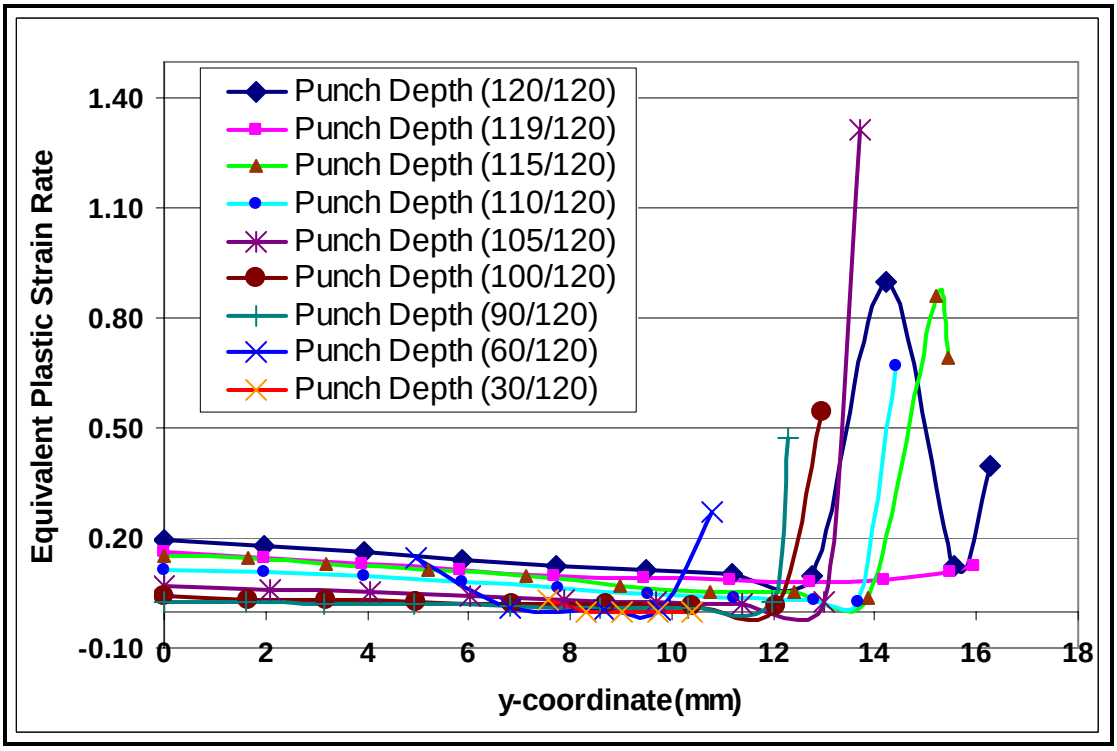

Figure 4.37 Variation of equivalent plastic strain rate with Levanov's friction model

Figure 4.38 shows the variation of von-Mises equivalent stress. Curve characteristics are in agreement with the results of General Friction Model results.

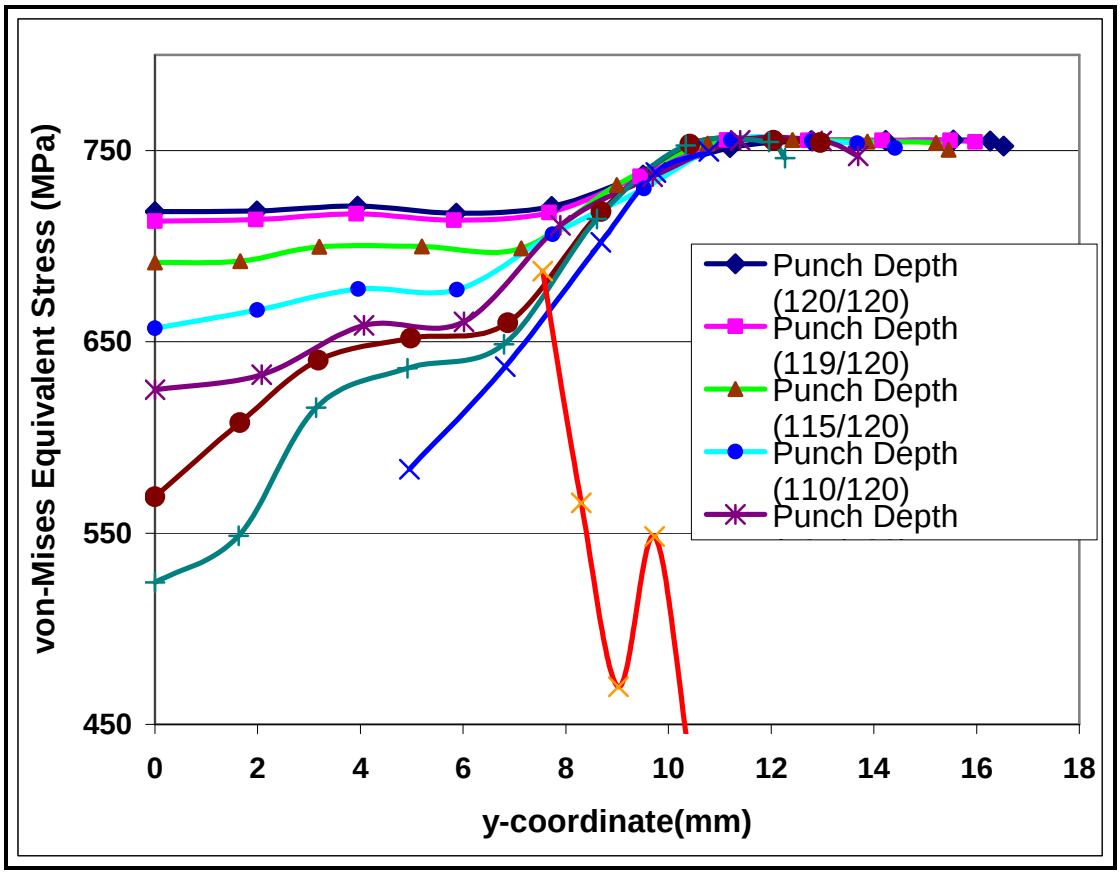

Figure 4.38 Variation of von-Mises equivalent stress with Levanov's friction model

4.3 Discussion for Case Study II

Similar to case study I, the variation of coefficient of friction is higher in Levanov's model than the Bay's General friction model. In order to enlighten this fact it will be useful to plot the variation of coefficient of friction with respect to the ratio of q/σ_0. Figure 4.39 shows the variation of friction coefficient in Bay's model while Figure 4.40 shows the variation of friction coefficient in Levanov's model. Note that these plots are independent from the case studies analyzed above.

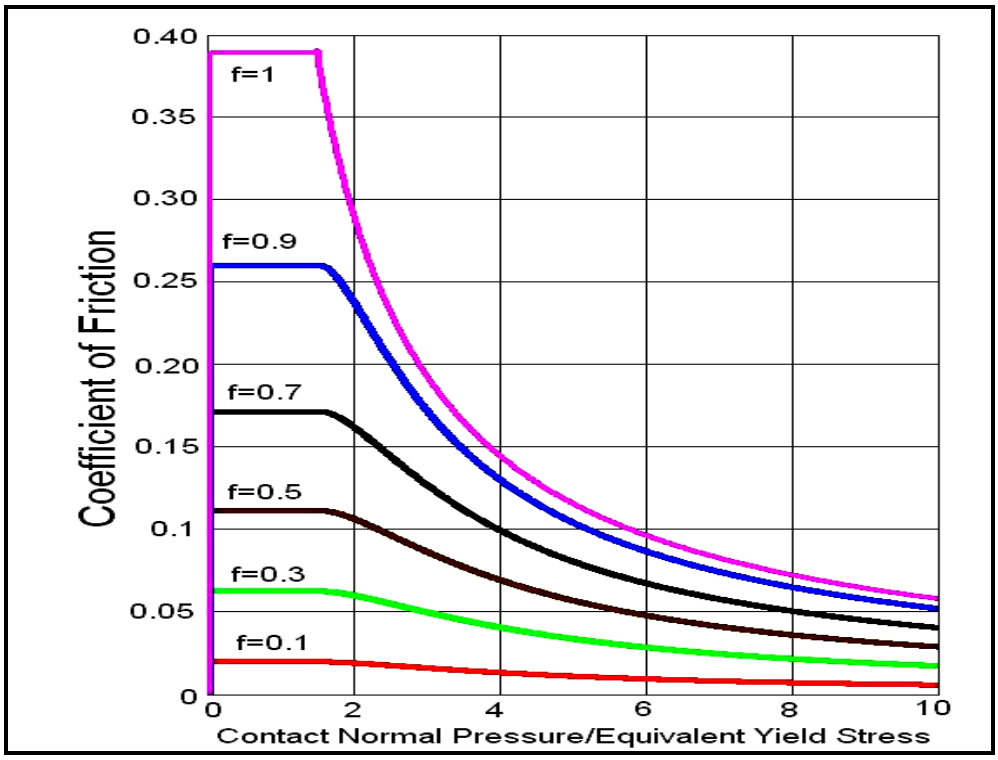

Figure 4.39 Variation of coefficient of friction in General friction model (Bay's)

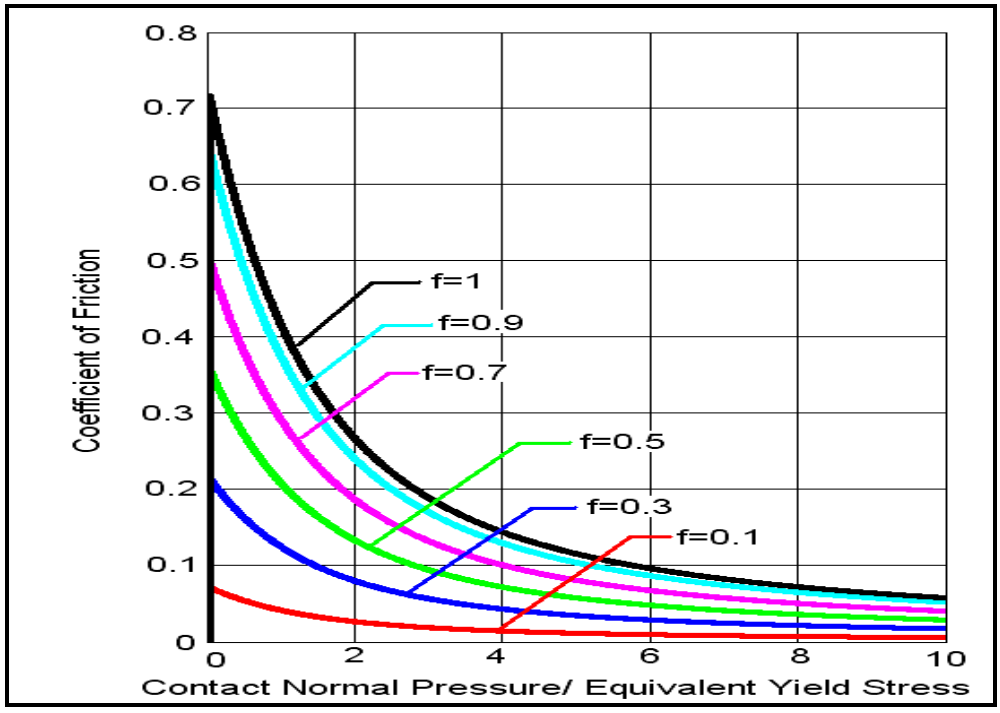

Figure 4.40 Variation of coefficient of friction in Levanov's model

The most significant difference between these variations is that the coefficient of friction values are constant in General friction model for $\left(q/\sigma_0\right)<1.5$. Figure 4.41 denotes the comparison of variation of friction coefficient in both models. In General Friction Model, up to a certain value of q/σ_0 (which is about 1.5) the coefficient of friction is constant while in Levanov's friction model the coefficient of friction decreases considerably from relatively high values.

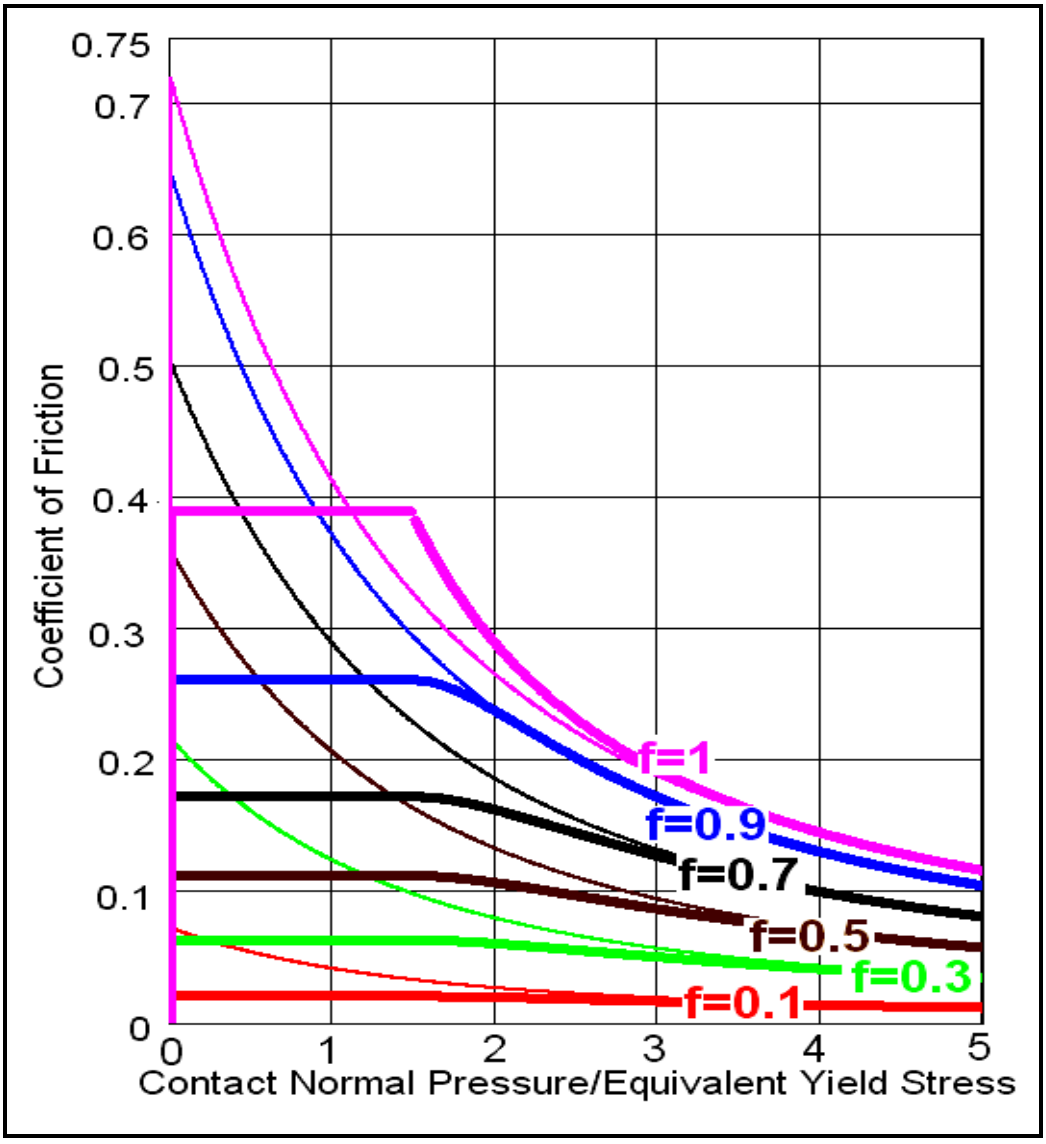

Figure 4.41 Comparison of coefficient of friction variation in General friction (Bay's) model (thick lines) and Levanov's friction model (thin lines)

Table 4.4 gives the maximum values of coefficient of frictions for both models for different friction factors. In Levanov's model the maximum values are reached at the ratio of $q/\sigma_0 = 0$, while in General Friction (Bay's) Model the maximum values are reached for the range $0 \le q/\sigma_0 \le 1.5$

Table 4.4 Maximum coefficient of friction values for friction models

Friction Factor Value	Maximum Value of Coefficient of Friction in Levanov's Model	Maximum Value of Coefficient of Friction in Bay's Model
f = 0.1	0.0719	0.019855
f = 0.3	0.2157	0.06262
f = 0.5	0.35949	0.11151
f = 0.7	0.50329	0.17155
f = 0.9	0.64709	0.26029
f = 1	0.71899	0.38898

In the second case study, the reason of choosing f = 0.3 is based on the range of coefficient of friction. In cold forging operations due to availability of lubricants the coefficient of friction varies between 0.05 and 0.1 which is comparatively small with respect to hot forming operations as given in Chapter 1. Therefore, considering the maximum values of coefficients given in Table 4.2, it was not reasonable to choose the friction factor value greater than 0.3. Although the maximum value of friction coefficient in Levanov's model for f = 0.3 is about 0.2157, it decreases rapidly with the increasing ratio of q/σ_0. For the ratio of 1.5, which can easily be obtained in forming operations as can be seen from the Figures 4.23 and 4.33, the coefficient of friction in Levanov's model is about 0.1. At that point the coefficient of friction value is about 0.06 in Bay's General Friction Model.

Except at low q/σ_0 ratios in friction models, both curves tend to converge to the same value at higher q/σ_0 ratios as can be seen from Figure 4.41.

CHAPTER V

CONCLUSIONS AND FUTURE WORKS

5.1 Conclusions

In this study, the two friction models giving variable coefficient of friction were integrated to commercially available finite element codes MSC SuperForm v.2004 and MSC Marc v.2003 to investigate the effects of variable coefficient of friction in cold forging process.

The followings are concluded from the finite element analyses of cold forging by using friction models which provide variable coefficient of friction values.

1) Although FEA package programs use standard constant coefficient of friction throughout the cold forming process, it was verified that the friction values could change significantly during the plastic deformation.

2) In cylinder upsetting, the pressure distribution is almost uniform on the surface and does not change all along the forging process for height reduction up to 67 %. It is observed that, constant friction models adequately model friction condition provided the proper coefficient of friction is determined. However, the other models could not reflect the actual friction condition sufficiently.

3) In bolt head forging, two variable coefficient of friction models were used and the pressure distribution was not uniform on the surface and changes all along the forging process for which the contact normal stress to equivalent yield stress ratio varies between 1 and 3.3.

4) It is observed that large variation on the coefficient of friction depends on the friction model used, the cold forged part geometry and the ratio of contact normal stress to equivalent yield stress.

5) In General friction and Levanov's friction models, the coefficient of friction values take their highest values for q/σ_0 ratio smaller than 1.5. The coefficient of friction values decrease with the increasing contact normal pressure.

6) For the contact normal stress to equivalent yield stress ratio higher than 4.0, the coefficient of friction values are almost same for both friction models.

5.2 Future Works

In this thesis two friction models are applied to two different upsetting geometries. The following future studies can be suggested:

- The friction models integrated into a commercial FEA model with variable coefficient of friction is to be applied to some other complex cold forging parts with large contact pressure variation on the contact interface between the die and the workpiece.

- Other friction models that take the effect of sliding velocity, surface roughness into consideration are to be compared with the friction models used in this thesis.

- In cold forging operations where the contact pressures are high, with the use of lubricants, boundary lubrication conditions occur and the models can be used to predict the coefficient of friction.

REFERENCES

[1] An educational tribology web site, http://www.tribology-abc.com/, Last Access Date:31.12.2004

[2] Colchero, J. et al. *"Friction on an Atomic Scale"* Handbook of Micro/Nanotribology (Ed. Bharat Bhushan), Boca Raton, CRC Press LLC, 1999

[3] Tan, X., *"Comparisons of Friction Models in Bulk Metal Forming",* Tribology International, v.35, pp. 385-393, 2002

[4] Kalpakjian, S., Schmid, S.R., *"Manufacturing Engineering and Technology"*, Chapter 32: Tribology: Friction, Wear and Lubrication, p.884, Prentice-Hall, 2001

[5] Bowden, F. P., Tabor, D., *"The Friction and Lubrication of Solids"*, Part I, Part II , Oxford University Press, London 1954, 1964,

[6] Wilson, W., *"Friction Models for Metal Forming in the Boundary Lubrication Regime"***,** Trans. ASME, Journal of Engineering Materials and Technology 1991, v.113, p.60-68

[7] Wilson, W.R.D., *"A Realistic Friction Model for Computer Simulation of Sheet Metal Forming Processes",* Journal of Engineering for Industry, 1995, Vol.117, pp 202-209

[7] Darendeliler, H., Akkök, M., Yücesoy, C.A., *"Effect of Variable Friction Coefficient on Sheet Metal Drawing",* Tribology International, 2002, v.35, pp.97-104

[8] Polycarpou, A.A., Soom, A., *"Boundary and Mixed Friction in the Presence of Dynamic Normal Loads: Part I- System Model",* Transactions of ASME, Journal of Tribology, 1995, v.117, p.255-261

[9] Polycarpou, A.A., Soom, A*., "Two-Dimensional Models of Boundary and Mixed Friction at a Line Contact",* Transactions of ASME, Journal of Tribology, 1995, v.117, p.178-185

[10] Polycarpou, A.A., Soom, A*., "Boundary and Mixed Friction in the Presence of Dynamic Normal Loads: Part I-System Model",* Transactions of ASME, Journal of Tribology, 1995, v.117, pp.255-260

[11] Polycarpou, A.A., Soom, A*., "Boundary and Mixed Friction in the Presence of Dynamic Normal Loads: Part II-Friction Transients",* Transactions of ASME, Journal of Tribology, 1995, v.117, pp.261-265

[12] Polycarpou, A.A., Soom, A., "*A Two-Component Mixed Friction Model for a Lubricated Line Contact",* Transactions of ASME, Journal of Tribology, 1996, v.118, p.183-189

[13] Wanheim, T., *"Friction at High Normal Pressures*", Wear, 25(1973), pp.225-244

[14] Wanheim, T., Bay, N., Petersen, A.S., "*A Theoretically Determined Model for Friction in Metal Working Processes"*, Wear, 28(1974), pp.251-258

[15] Petersen, S.B., Martins, P.A.F., Bay, N., *"Friction in Bulk Metal Forming: A General Friction Model vs. the Law of Constant Friction"*, Journal of Materials Processing Technology, 66 (1997), pp.186-194

[16] Torrance, A.A., Galligan J., Liraut G. *" A Model of the Friction of a Smooth Hard Surface Sliding Over a Softer One " ,* Wear, 1997, v.212, pp. 213-220

[17] Levanov, A.N., *"Improvement of Metal Forming Processes by means of Useful Effects of Plastic Friction"*, Journal of Materials Processing Technology, 1997, v.72, pp.314-316

[18] Hallström, J., *"Influence of Friction on Die Filling in Counterblow Hammer Forging",* Journal of Materials Processing Technology, 2000, v.108, pp.21-25

[19] D.A., Stephenson, *"Friction in Cold Strip Rolling"*, Wear 92 (1983), pp. 293-311

[20] Bay, N., Andreasen, J.L., Olsson, D.D., Massoni, E., Bariani, P., Dal Negro, T., Humi, P., Ducloux, R., Holmedal, B., *" Development of a 3D Finite Element code for Forging An overview of the Brite/Euram project EFFORTS", 2001,* 2nd International Conference on Design and Production of Dies and Molds, Kuşadası, Turkey.

[21] Male,A.T., Cockcroft, M.G., *" A Method for the Determination of the Coefficient of Friction of Metals under Conditions of Bulk Plastic Deformation"*, Journal of the Institute of Metals, Vol.93, pp.38-46, 1964-1965

[22] Cho, H.; Ngaile, G., *"Simultaneous Determination of Flow Stress and Interface Friction by Finite Element Based Inverse Analysis"*, 53rd CIRP General Assembly, August 24-30 2003 Montreal, Canada,

[23] Sofuoğlu, H., Gedikli, H., Rasty, J., *"Determination of Friction Coefficient by Employing the Ring Compression Test"*, Transactions of ASME, Journal of Engineering Materials and Technology, Vol. 123, 2001, pp. 338-348

[24] Petersen, S.B., Martins, P.A.F., Bay N., *"An Alternative Ring-Test Geometry for the Evaluation of Friction under Low Normal Pressure"*, Journal of Materials Processing Technology, 79(1998), pp. 14-24

[25] Sofuoğlu, H., Gedikli, H., *"Determination of Friction Coefficient Encountered in Large Deformation Processes"*, Tribology International, 35 (2002), pp.27-34

[26] Buschhausen, A., Weinmann, K., Altan, T., Lee, J.Y. *"Evaluation of Lubrication and Friction in Cold Forging Using a Double Backward-Extrusion Process"* Journal of Materials Processing Technology, 33(1992), pp.95-108

[27] Altan T., *"Cold Forging Technology in Global Competition"*, International Conference on "New Developments in Forging Technology", Fellbach/Stutgart, Germany, June 02-04, 2003.

[28] Forcellese, A., Gabrielli, A., Barcellona, A., Micari A., *"Evaluation of Friction in Cold Metal Forming"*, Journal of Materials Processing Technology, 45(1994), pp.619-624

[29] *"MSC Marc and MSC Marc Mentat, Release Guide Version 2003"*, MSC Software Corporation, 2003

[30] MSC Superform Version 2004, Marc Analysis Research Corporation, 2004

[31] *Compaq Visual FORTRAN Standard Edition 6.6.A,* Compaq Computer Corporation, 2001

[32] İsbir, S. Ş., *"Finite Element Analysis of Trimming"*, M.S. Thesis, 2002, p.24, Middle East Technical University, Ankara.

[33] *MSC.Marc Users's Guide Volume B: Element Library,* Marc Analysis Research Corporation, 2003

[34] *MSC.Marc User's Guide Volume D: User Subroutines and Special Routines,* Marc Analysis Research Corporation, 2003

[35] Bout, A., *"Advanced Marc Analyses Applying User Subroutines",* Publication of MARC Analysis Research Corporation-Europe

[36] Tan, X., *"Friction-reducing contact area expansion in upsetting"*, Proceeding of Institution of Mechanical Engineers, Vol.215 Part J pp.189-199

[37] SAAB Company, http://supplier.saab.com/std/docs/514212.pdf, Last Access Date: 31.12.2004

[38] MSC. *Marc Material Database,* Marc Analysis Research Corporation, 2003

APPENDIX A

SOURCE CODE OF THE USER-SUBROUTINES

User-Subroutine for Bay's General Friction Model (f=0.3)

```
      subroutine ufric(mibody,x,fn,vrel,temp,yiel,fric,
     +time,inc,nsurf)
      implicit real*8 (a-h,o-z)
      DIMENSION X(2),MIBODY(4),VREL(1),TEMP(2)
c-----------------------------------------------------------------------
c     GENERAL FRICTION MODEL- (PROPOSED BY WANHEIM&BAY)
C
C     Tn: Friction Stress   MPa
C     k: Yield Stress in pure shear  MPa
c     sigma: Equivalent Yield Stress  MPa
c     q: Contact Normal Stress=fn
c     f: Friction factor
C     alfa: Ratio of real area contact to the apparent area
C     qp, Tnp : are factors depend on f
C-----------------------------------------------------------------------
c     f must be entered
C     OUTPUT FILE IS OPENED FOR WRITING
      OPEN (3, FILE='29kas.txt')
      WRITE (3,*) 'mibody',mibody, inc
      WRITE (3,*) 'normal force or stress',fn, yiel
      WRITE (3,*) '------------------------------'
      if(inc.eq.1) then
      FRIC=0.1d0
      else
      ys=YIEL/SQRT(3.0d0)
      write(3,*) 'ys', ys
      sigma=YIEL
      write(3,*)'sigma=',sigma
      f=0.3d0
      A=1.0d0+(acos(-1.0d0)/2.0d0)+acos(f)+sqrt(1.0d0-f**2.0d0)
      B=sqrt(3.0d0)*(1+(sqrt(1.0d0-f)))
      qp=(sigma)*(A/B)
      D=1.0d0-(sqrt(1.0d0-f))
      Tnp=ys*D
      if(fn.le.qp) then
      Tn=ys*D*((fn/sigma)/(A/B))
      else
      Tn=ys*(D+(f-D)*(1.0d0-exp((D*((A/B)-(fn/sigma))/((A/B)*(f-D))))))
      end if
      FRIC=abs(Tn/fn)
      end if
      WRITE (3,*)  'increment no:', inc
      WRITE (3,*)  'frictional,normal stres:', Tn,fn
      WRITE (3,*)  'fric=', fric
      WRITE (3,*)  '----------------------------------------'
      return
      end
```

User-Subroutine for Levanov Friction Model (f=0.3)

```
      subroutine ufric(mibody,x,fn,vrel,temp,yiel,fric,
     +time,inc,nsurf)
      implicit real*8 (a-h,o-z)
      DIMENSION x(2),MIBODY(4),VREL(1),TEMP(2)
c-----------------------------------------------------------------------
c     LEVANOV'S FRICTION MODEL
C
C     Tn: Friction Stress   MPa
C     k: Yield Stress in pure shear  MPa
c     sigma: Equivalent Yield Stress  MPa
c     q: Contact Normal Stress
c     f: Friction factor
C     alfa: Ratio of real area contact to the apparent area
C     qp, Tnp : are factors depend on f
C-----------------------------------------------------------------------
C     f must be entered

C     OUTPUT FILE IS OPENED FOR WRITING
      OPEN (3, FILE='25kas2')
C     write(3,*) 'yield',YIEL
C     if(inc.eq.18.or.inc.eq.19)then
      WRITE (3,*) 'mibody',mibody
      WRITE (3,*) 'updated coordinates',x
      WRITE (3,*) 'normal force or stress',fn
      WRITE (3,*) 'relative velocity',vrel
      WRITE (3,*) 'temperature',temp
      WRITE (3,*) 'flow stress',yiel
      WRITE (3,*) 'time',time
      WRITE (3,*) 'increment no',inc
      WRITE (3,*) 'surface being contacted',nsurf
      WRITE (3,*) '------------------------------'
      if(inc.eq.1) then
      FRIC=0.1d0
      else
      ys=YIEL/SQRT(3.0d0)
      write(3,*) 'ys', ys
      sigma=YIEL
      write(3,*)'sigma=',sigma
      f=0.3d0
      Tn=ys*f*(1.0d0-exp(-1.25d0*(fn/sigma)))
      FRIC=abs(Tn/fn)
      end if
      WRITE (3,*)  'incremet no:', inc
      WRITE (3,*)  'friction stres:', Tn
      WRITE (3,*)  'normal stress:', fn
      WRITE (3,*)  'fric=', fric
      WRITE (3,*)  '-----------------------------------------'
      return
      end
.
```

The original UFRIC subroutine is written with the following headers

```
SUBROUTINE UFRIC
(MIBODY,X,FN,VREL,TEMP,YIEL,FRIC,TIME,INC,NSURF)
IMPLICIT REAL *8 (A-H, O-Z)
DIMENSION X(2),MIBODY(4),VREL(1),TEMP(2)
   user coding
RETURN
END
```

where:

Input:

For distributed friction based on nodal stresses:

MIBODY (1) is your element number.

MIBODY (2) is the side number.

MIBODY (3) is the surface integration point number.

MIBODY (4) is the internal element number.

For nodal friction based on nodal forces:

MIBODY (1) is your node number.

MIBODY (2) is not used; enter 0.

MIBODY (3) is not used; enter 0.

MIBODY (4) is the internal node number.

X is the updated coordinates of contact point where friction is being calculated.

FN is the normal stress/force being applied at that point.

VREL is the relative sliding velocity at contact point.

TEMP1 is the temperature of contact point.

TEMP2 is the voltage of contact point (Joule heating).

YIEL is the flow stress of workpiece material at contact point.

TIME is the current time.

INC is the increment number.

NSURF is the surface being contacted by the side for which friction calculations are being made.

Required Output:

FRIC is the friction coefficient or friction factor to be provided by the user.